Available online at www.sciencedirect.com
SCIENCE DIRECT
ELSEVIER
Colloids and Surfaces A: Physicochem. Eng. Aspects 282–283 (2006) 143–161
COLLOIDS AND SURFACES A
www.elsevier.com/locate/colsurfa

Micellar surfactant solutions: Dynamics of adsorption at fluid interfaces subjected to stationary expansion

Krassimir D. Danov [a], Peter A. Kralchevsky [a,*], Kavssery P. Ananthapadmanabhan [b], Alex Lips [b]

[a] *Laboratory of Chemical Physics and Engineering, Faculty of Chemistry, University of Sofia, 1164 Sofia, Bulgaria*
[b] *Unilever Research & Development, Trumbull, CT 06611, USA*

Received 15 August 2005; received in revised form 17 October 2005; accepted 21 October 2005
Available online 6 January 2006

Dedicated to Professor Ivan B. Ivanov (LCPE, University of Sofia) on the occasion of his 70th birthday.

Abstract

Here, we consider a micellar surfactant solution whose surface is subjected to stationary expansion. The adsorption at the fluid interface gives rise to diffusion of surfactant monomers and micelles, and to release of monomers by the micelles. To describe this process, we applied a recently derived general system of four ordinary differential equations, which are linearized for the case of small perturbations. The numerical solution of the problem reveals the existence of four distinct kinetic regimes. At the greatest expansion rates, the surfactant adsorption is affected by the fast micellar process (regime AB). At lower expansion rates, the fast process equilibrates and the adsorption occurs under diffusion control (regime BC). With the further decrease of the expansion rate, the surfactant adsorption is affected by the slow micellar process (regime CD). Finally, at the lowest expansion rates, both the fast and slow micellar processes are equilibrated, and the adsorption again occurs under diffusion control (regime DE). For each separate kinetic regime, convenient analytical expressions for the dynamic surface tension and adsorption are derived. At low micelle concentrations, "rudimentary" kinetic diagrams are observed, which are characterized by merging or disappearance of the regimes BC and CD. Usually, only one of the kinetic regimes is experimentally detected. The developed theoretical model enables one to identify which of the four regimes is observed in a given experiment, and to interpret properly the obtained data. We applied the model to process available data for the nonionic surfactant Brij 58, and for two cationic surfactants, C_{14}TAB and C_{16}TAB. Good agreement between theory and experiment is achieved.

Keywords: Micellar surfactant solutions; Fast and slow micellization processes; Surfactant adsorption kinetics; Dynamic surface tension; Diffusion in micellar solutions; Strip method; Overflowing cylinder method

1. Introduction

The diffusion and convective transport of monomers and aggregates in surfactant solutions is accompanied by release or uptake of monomers by the micelles. The first models of micellar kinetics in spatially uniform solutions have been developed by Kresheck et al. [1], and Aniansson and Wall [2]. The existence of "fast" and "slow" processes of the micellar dynamics has been established. The experimental techniques for investigation of the surfactant self-assembly have been reviewed in a recent book [3]. Detailed reviews on micellar kinetics and dynamic surface tension have been published by Noskov and Grigoriev [4], and Noskov [5].

The first theoretical model of surfactant adsorption from micellar solutions was proposed by Lucassen [6] in relation to the analysis of tensiometric data from experimental methods with oscillating surface area [7]. This model uses the simplifying assumptions that the micelles are monodisperse, and that the micellization happens as a single step, which is described as a reversible reaction of order n (the micelle aggregation number). This nonlinear problem was linearized for the case of small perturbations, and the assumption for local quasi-equilibrium between micelles and monomers was employed [6,8–10]. The nonlinear problem was solved numerically by Miller [11] and analytically by Breward and Howell [12], again using the assumption for monodisperse micelles. An alternative

* Corresponding author. Tel.: +359 2 9625310; fax: +359 2 9625643.
E-mail address: pk@lcpe.uni-sofia.bg (P.A. Kralchevsky).

0927-7757/$ – see front matter © 2005 Elsevier B.V. All rights reserved.
doi:10.1016/j.colsurfa.2005.10.090

approach to the nonlinear problem, based on the von Karman's method, was proposed in [13]. More realistic models for the diffusion in micellar solutions, which account for the polydispersity of the micelles and the multi-step character of the micellar process, were developed independently by Noskov [14], Johner and Joanny [15], and Dushkin et al. [16,17].

In the model [6], the assumption for a complete local dynamic equilibrium between monomers and micelles makes possible to use the equilibrium mass-action law for the micellization reaction. In such a case, the surfactant transfer corresponds to a conventional diffusion-limited adsorption characterized by an apparent diffusion coefficient, D_A, which depends on the micelle diffusivity, concentration and aggregation number [8,9]. D_A is independent of the rate constants of the fast and slow micellar processes: k_m^- and k_S^-. Correspondingly, if the quasi-equilibrium model [6] is applicable to a given experimental situation, then k_m^- and k_S^- cannot be determined from the obtained data for the dynamic surface tension or adsorption.

Later, Joos et al. [8–10,18] confirmed experimentally that in some cases the adsorption from micellar solutions can be actually described as a diffusion-limited process characterized by an apparent diffusivity, D_A, but the experimental data were not in agreement with the expression for D_A from [6]. An alternative semiempirical expression for D_A was proposed [8,9], which agrees well with the experiment, but lacks a theoretical basis. In subsequent studies, Joos et al. [10,19] established that sometimes the dynamics of adsorption from micellar solutions exhibits a completely different kinetic pattern: the interfacial relaxation is exponential, rather than inverse-square-root, as it is for the diffusion-limited kinetics. The theoretical developments [10,19,20] revealed that the exponential relaxation is influenced by the kinetics of the micellization processes, and from its analysis one could determine the rate constant of the fast process, k_m^-. The observation of different kinetic regimes for different surfactants and/or methods makes the physical picture rather complicated.

Recently, we proposed a theoretical model, which generalizes previous models of micellization kinetics in several aspects [21]. We avoided the use of the quasi-equilibrium approximation (local chemical equilibrium between micelles and monomers). The theoretical problem was reduced to a system of four nonlinear differential equations. Its solution gives the concentration of surfactant monomers, the total micelle concentration, the mean aggregation number, and the micelle polydispersity as functions of the spatial coordinates and time.

In a subsequent study [22], we applied the theoretical model from reference [21] to the case of surfactant adsorption at a quiescent interface, i.e. to the relaxation of surface tension and adsorption after a small initial perturbation. Computer modeling of the adsorption process was carried out. This analysis revealed the existence of four different relaxation regimes (stages) for a given micellar solution: Regime AB: adsorption influenced by the *fast* micellar process; Regime BC: *diffusion-limited* adsorption at equilibrated fast micellar process, but negligible slow micellar process; Regime CD: adsorption influenced by the *slow* micellar process; and Regime DE: *diffusion-limited* adsorption at equilibrated *both* the fast and slow micellar processes [22].

Experimentally, depending on the specific surfactant and method, one usually registers only one of the above regimes. Therefore, to interpret properly the data, one has to identify which of the four kinetic regimes is observed in the respective experiment. In particular, it was established [22] that the exponential relaxation of the surface tension, detected and investigated in references [19,20], corresponds to the regime AB. The diffusion-limited adsorption observed in the experiments by Joos et al. [8,9], is consistent with the regime BC. On the other hand, the diffusion-limited adsorption in the study by Lucassen [6], corresponds to the regime DE.

In general, the form of the theoretical expressions, and the shape of the kinetic diagrams depend on the type of the interfacial dynamics used in a given experimental method. In this respect, at least four groups of experimental methods could be identified: (i) *initial interfacial perturbation*: the fast formed drop method [23,24] and the inclined plate method [10,19,25]; (ii) *stationary expansion*: the strip method [10,26], the overflowing cylinder (OFC) [27–31], and the Langmuir trough at constant expansion rate [10]; (iii) *non-stationary expansion*: the dynamic drop volume method [8,18], the maximum-bubble-pressure method [32–35], and the expanding-drop method [36,37]; and (iv) methods with *oscillating surface area* [6,7,38–41].

In [22] we considered the theoretical description in relation to the first group of experimental methods, those with adsorption at a quiescent interface, after an initial perturbation. Here, our aim is to apply the general theory from reference [21] to analyze the second group of methods, viz. the methods with stationary expansion of a fluid interface [10,26–31]. The paper is organized as follows.

In Section 2 we give a brief overview of the basic dynamic equations for surfactant concentrations below the critical micellization concentration (CMC) for the case of stationary interfacial expansion. In Section 3, we formulate the basic equations for micellar solutions, and their special form in the case of stationary expansion. The theory is simpler in terms of the total (integral) perturbations, which are considered in Section 4. Numerical results are presented in the form of kinetic diagrams. The four kinetic regimes, AB, BC, CD, and DE, are identified and discussed. Next, in Section 5, analytical expressions describing the dependence of adsorption on the interfacial expansion rate are derived for each of the four regimes. Section 6 is devoted to the "rudimentary" kinetic diagrams, which are observed at low micelle concentrations. Finally, in Section 7 we apply the theoretical model to fit three sets of available experimental data for dynamic surface tension and adsorption obtained by means of the strip and OFC methods. It is interesting to note that the experimental data complies with the regime BC for the considered experiments.

2. Concentrations below the CMC: basic equations

When a fluid interface is subjected to uniform expansion and/or compression, the interfacial area becomes a function of time, $A = A(t)$. The rate of surface dilatation, $\dot{\alpha}(t)$, and the surface

dilatation, $\alpha(t)$, are defined as follows, see e.g. [10,42]:

$$\dot{\alpha}(t) \equiv \frac{1}{A}\frac{\mathrm{d}A}{\mathrm{d}t} = \frac{\mathrm{d}\alpha(t)}{\mathrm{d}t}, \qquad \alpha(t) = \int_0^t \dot{\alpha}\,\mathrm{d}t = \ln\frac{A(t)}{A(0)} \tag{2.1}$$

Under *stationary* interfacial dilatation (or compression), we have $\dot{\alpha} = \text{const}$. In this case, the interfacial dilatation induces surfactant diffusion and adsorption, which are described by the equations [9,10]:

$$-\dot{\alpha}z\frac{\mathrm{d}c_{1,\mathrm{p}}}{\mathrm{d}z} = D_1\frac{\mathrm{d}^2c_{1,\mathrm{p}}}{\mathrm{d}z^2} \tag{2.2}$$

$$\dot{\alpha}\Gamma_{\mathrm{eq}} = D_1\left.\frac{\mathrm{d}c_{1,\mathrm{p}}}{\mathrm{d}z}\right|_{z=0} \tag{2.3}$$

Here and hereafter, the subscripts "eq" and "p" denote equilibrium value and perturbation of the respective parameter of the system. Thus, $c_{1,\mathrm{p}} = c_1(z,t) - c_{1,\mathrm{eq}}$ is the perturbation in the concentration of the surfactant monomers, c_1; as usual, t is time, and z is coordinate normal to the interface; the latter is located at $z=0$; Γ and D_1 denote surfactant adsorption and diffusivity. Because we are dealing with a stationary process, the derivatives $\partial c_{1,\mathrm{p}}/\partial t$ and $\mathrm{d}\Gamma/\mathrm{d}t$ in Eqs. (2.2) and (2.3) are missing. In addition, the convective term in Eq. (2.2) is expressed by using the approximation of van Voorst Vader et al. [43], $\mathbf{v}\cdot\nabla c_{1,\mathrm{p}} = -\dot{\alpha}z(\partial c_{1,p}/\partial z)$, where $\mathbf{v}$ is velocity; see also [13,44]. The validity of this approximation has been mathematically proven in [12,45,46]. This approximation is based on the fact that in most of the liquids, the thickness of the diffusion boundary layer is much smaller than the thickness of the hydrodynamic boundary layer. For $\dot{\alpha} = \text{const.}$, using the boundary condition (2.3), one obtains the first integral of Eq. (2.2) [9,10]:

$$\frac{\mathrm{d}c_{1,\mathrm{p}}}{\mathrm{d}z} = \frac{\Gamma_{\mathrm{eq}}\dot{\alpha}}{D_1}\exp\left(-\frac{\dot{\alpha}z^2}{2D_1}\right) \tag{2.4}$$

The integration of Eq. (2.4) with respect to z from zero to infinity yields the subsurface (at $z=0$) value of the surfactant concentration [9]:

$$c_{1,\mathrm{p}}(0) = -\Gamma_{\mathrm{eq}}\left(\frac{\pi\dot{\alpha}}{2D_1}\right)^{1/2} \tag{2.5}$$

In the case of small deviations from equilibrium, the perturbation in adsorption, $\Gamma_{\mathrm{p}} = \Gamma - \Gamma_{\mathrm{eq}}$, is related to the perturbation in the subsurface surfactant concentration, $c_{1,\mathrm{p}}(0)$, as follows:

$$\Gamma_{\mathrm{p}} = h_{\mathrm{a}}c_{1,\mathrm{p}}(0), \qquad h_{\mathrm{a}} \equiv \left(\frac{\partial\Gamma}{\partial c_1}\right)_{\mathrm{eq}} \tag{2.6}$$

where h_{a} is the so-called adsorption length, which is calculated from the equilibrium adsorption isotherm, $\Gamma = \Gamma(c_1)$. For micellar solutions, h_{a} should be estimated at the critical micelle concentration, i.e. at $c_{1,\mathrm{eq}} = \mathrm{CMC}$.

The combination of Eqs. (2.5) and (2.6) leads to a square-root dependence of Γ_{p} on $\dot{\alpha}$:

$$\frac{\Gamma_{\mathrm{eq}} - \Gamma}{\Gamma_{\mathrm{eq}}} = \left(\frac{\pi\dot{\alpha}h_{\mathrm{a}}^2}{2D_1}\right)^{1/2} \tag{2.7}$$

To relate the dynamic surface tension, γ, to $\dot{\alpha}$, we will use the Gibbs adsorption equation, $\mathrm{d}\gamma = -\Gamma kT\,\mathrm{d}\ln c_1$, where T is the temperature, and k is the Boltzmann constant. For small deviations from equilibrium, the latter equation yields:

$$\gamma - \gamma_{\mathrm{eq}} = -\Gamma_{\mathrm{eq}}kT\frac{c_{1,\mathrm{p}}(0)}{c_{1,\mathrm{eq}}} \tag{2.8}$$

Then, the combination of Eqs. (2.5) and (2.8) leads to [9]:

$$\frac{\gamma - \gamma_{\mathrm{eq}}}{kT} = \frac{\Gamma_{\mathrm{eq}}^2}{c_{1,\mathrm{eq}}}\left(\frac{\pi\dot{\alpha}}{2D_1}\right)^{1/2} \tag{2.9}$$

3. Concentrations above the CMC: basic system of equations

3.1. General form of the linearized boundary problem

As in the previous section, we consider the general case of a planar fluid interface, which is subjected to uniform expansion or compression, characterized by the rate of surface dilatation, $\dot{\alpha}(t)$. Here, one of the two neighboring fluid phases is assumed to be a micellar surfactant solution. As known [2–5], the micelle size distribution exhibits three different regions (Fig. 1): (i) region of the monomers and oligomers, Ω_{o} $(1 \le s \le n_{\mathrm{o}})$; (ii) region of the rare aggregates, Ω_{r} $(n_{\mathrm{o}} < s < n_{\mathrm{r}})$, and (iii) region of the abundant (typical) micelles, Ω_{m} $(s \ge n_{\mathrm{r}})$. In the region Ω_{r}, the aggregate concentration is assumed to be relatively small (Fig. 1). In the region Ω_{m}, the peak of the micelle size distribution is usually described by a Gaussian curve [2]:

$$c_s = \frac{C_{\mathrm{m}}}{\sqrt{2\pi}\sigma}\exp\left[-\frac{(s-m)^2}{2\sigma^2}\right] \quad (s \ge n_{\mathrm{r}}) \tag{3.1}$$

Here C_{m} is the total concentration of the abundant micelles; m is their mean aggregation number; σ^2 is the dispersion of the Gaussian distribution, which characterizes the polydispersity of the abundant micelles. We assume that Eq. (3.1) holds under both equilibrium and dynamic conditions. In the latter case, the parameters in Eq. (3.1) depend on the spatial coordinate, z, and time, t, i.e. we have: $C_{\mathrm{m}}(z,t)$, $m(z,t)$ and $\sigma(z,t)$.

The dilatation of the fluid interface gives rise to surfactant adsorption and diffusion. Both surfactant monomers and

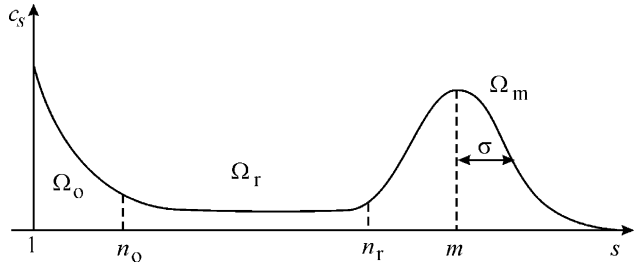

Fig. 1. Sketch of the typical size distribution of aggregates in a surfactant solution; c_s and s are the aggregate concentration and aggregation number; Ω_{o}, Ω_{r} and Ω_{m} are, respectively, the regions of oligomers, rare aggregates and abundant micelles; n_{o} and n_{r} represent boundaries between the regions; $s = m$ corresponds to the peak in the region Ω_{m}.

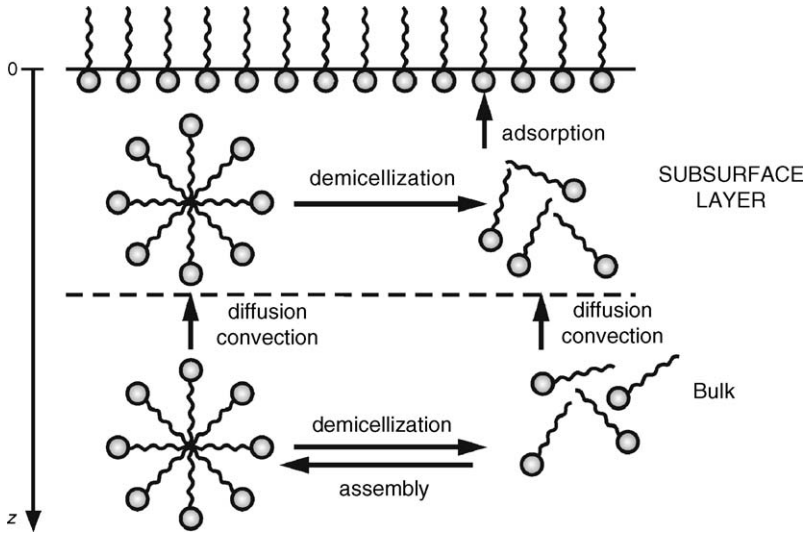

Fig. 2. Process of surfactant adsorption from micellar solutions. In the neighborhood of an expanded adsorption monolayer, the micelles release monomers to restore the equilibrium surfactant concentration at the surface and in the bulk. The concentration gradients give rise to bulk diffusion of both monomers and micelles.

aggregates take part in the diffusion. The aggregates (micelles) exchange monomers between each other and with the surrounding solution (Fig. 2). This complex process can be adequately described by four functions of z and t [21]. These are the concentration of surfactant monomers, $c_1(z,t)$, and the three parameters of the micelle distribution, Eq. (3.1), viz. $C_m(z,t)$; $m(z,t)$, and $\sigma(z,t)$, see Fig. 1. A full system of nonlinear differential equations for determining the latter four functions has been derived in [21]. For small deviations from equilibrium (small perturbations), this system of equations, expressed in terms of the *perturbations*, can be linearized; see Eqs. (2.4), (2.22)–(2.23) and (3.3)–(3.6) in [21]:

$$\frac{\partial c_{1,p}}{\partial t} - \dot{\alpha} z \frac{\partial c_{1,p}}{\partial z} = D_1 \frac{\partial^2 c_{1,p}}{\partial z^2} - (m_{eq} - w\sigma_{eq})J - J_{m,0} \tag{3.2}$$

$$\frac{\partial C_{m,p}}{\partial t} - \dot{\alpha} z \frac{\partial C_{m,p}}{\partial z} = D_m \frac{\partial^2 C_{m,p}}{\partial z^2} + J \tag{3.3}$$

$$\frac{\partial m_p}{\partial t} - \dot{\alpha} z \frac{\partial m_p}{\partial z} = D_m \frac{\partial^2 m_p}{\partial z^2} - \frac{w m_{eq}\sigma_{eq}}{\beta c_{1,eq}} J + \frac{m_{eq}}{\beta c_{1,eq}} J_{m,0} \tag{3.4}$$

$$\frac{\partial \sigma_p}{\partial t} - \dot{\alpha} z \frac{\partial \sigma_p}{\partial z} = D_m \frac{\partial^2 \sigma_p}{\partial z^2} + (w^2 - 1)\frac{\sigma_{eq} m_{eq}}{2\beta c_{1,eq}} J - \frac{m_{eq} J_{m,0}}{2\beta c_{1,eq}\sigma_{eq}} - \frac{2k_m^-}{\sigma_{eq}^2}\sigma_p \tag{3.5}$$

Here we use the same notations as in reference [21]; we have set $S \approx 1$, see Eqs. (3.2) and (3.3) in [21], because the concentration of the surfactant monomers is much greater than that of the oligomers. As before, the subscripts "eq" and "p" mark the equilibrium values and the perturbations of the respective variables; see the comments after Eq. (2.3); D_m is the diffusion coefficient of the micelles; $J_{m,0}$ and J are reaction fluxes due, respectively, to the fast and slow micellar processes [21]:

$$J_{m,0} = k_m^- C_{m,eq}\left(\frac{c_{1,p}}{c_{1,eq}} + \frac{\sigma_p - \sigma_{eq} m_p}{\sigma_{eq}^3}\right) \tag{3.6}$$

$$\frac{J}{k_S^- c_{1,eq}} = (m_{eq} - w\sigma_{eq})\frac{c_{1,p}}{c_{1,eq}} - \frac{m_{eq} C_{m,p}}{\beta c_{1,eq}} + \frac{w m_p}{\sigma_{eq}} - (w^2 - 1)\frac{\sigma_p}{\sigma_{eq}} \tag{3.7}$$

Here, k_m^- is the rate constant of monomer dissociation from the micelles; k_S^- is the rate constant of the slow micelle relaxation process, see Eq. (4.26) in [21]. The parameter β in Eqs. (3.4)–(3.7) is the equilibrium concentration of surfactant in micellar form, scaled by the critical micellization concentration, CMC:

$$\beta \equiv \frac{(C_{tot} - CMC)}{CMC} = \frac{m_{eq} C_{m,eq}}{c_{1,eq}} \tag{3.8}$$

C_{tot} is the total surfactant concentration and the monomeric concentration is $c_{1,eq} = CMC$. Another equilibrium dimensionless parameter is

$$w \equiv \frac{(m_{eq} - n_r)}{\sigma_{eq}} > 1 \tag{3.9}$$

where n_r is aggregation number at the boundary between the regions of the rare aggregates and the abundant micelles at equilibrium (Fig. 1); σ_{eq} is the polydispersity of the equilibrium micelle size distribution. The convective terms in Eqs. (3.2)–(3.5), those containing $\dot{\alpha}$, are obtained by using the approximation of van Voorst Vader et al. [43], see Section 2.

In view of Eqs. (3.6) and (3.7), Eqs. (3.2)–(3.5) form a system of four linear differential equations for determining the evolution of the perturbations in the four basic parameters of the micellar system: $c_{1,p}(z,t)$; $C_{m,p}(z,t)$; $m_p(z,t)$, and $\sigma_p(z,t)$. To solve this

problem, we need boundary conditions at the interface ($z=0$) and in the bulk of solution ($z\to\infty$). Based on experimental results, it is usually accepted that the micelles do not adsorb at the fluid interface, and that only the monomers can adsorb [10,11]. These assumptions lead to the following mass balance equations at the interface:

$$\frac{\partial \Gamma_p}{\partial t} + \dot{\alpha}\Gamma_{eq} = D_1 \frac{\partial c_{1,p}}{\partial z} \quad \text{at} \quad z=0 \ \text{ and } \ t>0 \tag{3.10}$$

$$\frac{\partial C_{m,p}}{\partial z} = 0, \quad \frac{\partial m_p}{\partial z} = 0, \quad \frac{\partial \sigma_p}{\partial z} = 0 \quad \text{at}$$
$$z=0 \ \text{ and } \ t>0 \tag{3.11}$$

Eq. (3.10) is a generalization of Eq. (2.3). What concerns the other limit, $z\to\infty$, the perturbations $c_{1,p}(z,t)$; $C_{m,p}(z,t)$; $m_p(z,t)$, and $\sigma_p(z,t)$ are assumed to vanish in this limit (in the bulk of solution).

To close the set of boundary conditions, we have to specify the mechanism of surfactant adsorption. Here we will assume that the adsorption occurs under diffusion control. In this case, the subsurface layer of the solution is assumed to be in equilibrium with the adsorption layer at the interface. Then, the adsorption is related to the subsurface concentration of monomers by means of the equilibrium adsorption isotherm. For small perturbations, this isotherm is given by Eq. (2.6).

The general system of equations and boundary conditions, formulated in the present section, can be applied to describe the surfactant adsorption under various dynamic regimes, corresponding to different experimental methods. For example, such regimes could correspond to quiescent, expanding, or oscillating interface. The different dynamic regimes have different characteristic times, and correspond to different modified versions of the basis system of equations; therefore, they demand separate treatment. In this paper, we will focus our attention on the detailed investigation of the surfactant adsorption at a fluid interface subjected to stationary expansion, $\dot{\alpha}=$ const., see the next section.

3.2. Case of stationary expansion

In the case of surfactant adsorption at a fluid interface subjected to stationary expansion, it is convenient to introduce the following dimensionless quantities:

$$\zeta \equiv \frac{z}{h_a}, \quad \theta \equiv \frac{h_a^2}{D_1}\dot{\alpha}, \quad K_s \equiv \frac{h_a^2}{D_1}k_S^-, \quad K_m \equiv \frac{h_a^2}{D_1}k_m^- \tag{3.12}$$

Here, ζ, θ, K_s, and K_m are the dimensionless normal coordinate, z; expansion rate, $\dot{\alpha}$, and rate constants of the slow and fast micellar processes, k_S^- and k_m^-; see [21] for details. Furthermore, it is convenient to scale the dependent variables as follows:

$$\xi_1 \equiv -\frac{h_a}{\Gamma_{eq}}c_{1,p}, \quad \xi_c \equiv -\frac{h_a}{\Gamma_{eq}\beta}C_{m,p}, \quad \xi_m \equiv -\frac{h_a c_{1,eq}}{\Gamma_{eq}\sigma_{eq}^2}m_p,$$
$$\xi_\sigma \equiv -\frac{h_a c_{1,eq}}{\Gamma_{eq}\sigma_{eq}}\sigma_p \tag{3.13}$$

Here, ξ_1, ξ_c, ξ_m, and ξ_σ are the dimensionless *perturbations* in the concentration of surfactant monomers, $c_{1,p}$; micelle concentration, $C_{m,p}$; micelle mean aggregation number, m_p, and polydispersity of the abundant micelles, σ_p. The negative sign in Eq. (3.13) is chosen to make ξ_1, ξ_c, and ξ_m positive by definition.

It is important to note that the convenient definitions of the dimensionless perturbations ξ_1, ξ_c, ξ_m, and ξ_σ are different for different dynamic problems. Here, and in references [21,22], we are using the same notation for the dimensionless perturbations of the same variables, despite some differences in the used scaling. This should not lead to any misunderstandings, because the treatment of different dynamic problems is completely independent here and in references [21,22].

Because we are dealing with a steady-state process, the perturbations, ξ_i, are independent of time, but they are dependent on the dimensionless spatial coordinate, ζ; in other words, $\xi_i=\xi_i(\zeta)$, $i=1,c,m,\sigma$. In view of Eqs. (2.6), (2.8) and (3.13), the dimensionless perturbation in the subsurface concentration of monomers, $\xi_{1,0}\equiv\xi_1(\zeta=0)$, is related to the perturbations in the surfactant adsorption, Γ, and surface tension, γ, as follows:

$$\frac{\Gamma_{eq}-\Gamma}{\Gamma_{eq}} = \frac{c_{1,eq}h_a}{\Gamma_{eq}^2 kT}(\gamma-\gamma_{eq}) = \xi_{1,0} \tag{3.14}$$

For micellar solutions, the concentration, $c_{1,eq}$, the adsorption, Γ_{eq}, and the adsorption length, h_a, are to be calculated at the CMC. In view of Eqs. (3.12) and (3.13), for a stationary process Eqs. (3.2)–(3.5) acquire the form:

$$-\theta\zeta\frac{d\xi_1}{d\zeta} = \frac{d^2\xi_1}{d\zeta^2} - (m_{eq}-w\sigma_{eq})K_s\varphi_s - \frac{\beta K_m}{m_{eq}}\varphi_m \tag{3.15}$$

$$-\theta\zeta\frac{d\xi_c}{d\zeta} = B_m\frac{d^2\xi_c}{d\zeta^2} + \frac{K_s}{\beta}\varphi_s \tag{3.16}$$

$$-\theta\zeta\frac{d\xi_m}{d\zeta} = B_m\frac{d^2\xi_m}{d\zeta^2} - K_s\frac{w m_{eq}}{\beta\sigma_{eq}}\varphi_s + \frac{K_m}{\sigma_{eq}^2}\varphi_m \tag{3.17}$$

$$-\theta\zeta\frac{d\xi_\sigma}{d\zeta} = B_m\frac{d^2\xi_\sigma}{d\zeta^2} + K_s(w^2-1)\frac{m_{eq}}{2\beta}\varphi_s$$
$$-\frac{K_m}{2\sigma_{eq}^2}\varphi_m - \frac{2K_m}{\sigma_{eq}^2}\xi_\sigma \tag{3.18}$$

where $B_m\equiv D_m/D_1$, and the reaction fluxes, $J_{m,0}$ and J in Eqs. (3.6)–(3.7), are also expressed in dimensionless form:

$$\varphi_m \equiv \frac{h_a^3 m_{eq} J_{m,0}}{\Gamma_{eq}D_1K_m\beta} = \xi_1 - \xi_m + \frac{\xi_\sigma}{\sigma_{eq}^2} \tag{3.19}$$

$$\varphi_s \equiv \frac{h_a^3 J}{\Gamma_{eq}D_1K_s} = (m_{eq}-w\sigma_{eq})\xi_1 - m_{eq}\xi_c$$
$$+ w\sigma_{eq}\xi_m - (w^2-1)\xi_\sigma \tag{3.20}$$

Eq. (3.19) shows that if $\xi_\sigma\approx 0$ and $\xi_1\approx\xi_m$, then $\varphi_m\approx 0$, i.e. the system is equilibrated with respect to the *fast* micellar process, $J_{m,0}\approx 0$. In addition, Eq. (3.20) implies that if $\xi_\sigma\approx 0$, and

$\xi_1 \approx \xi_c \approx \xi_m$, then $\varphi_s \approx 0$, i.e. the system is equilibrated with respect to the *slow* micellar process, $J \approx 0$.

With the help of Eqs. (3.12)–(3.13), setting $\partial\Gamma/\partial t = 0$, we obtain the dimensionless form of the boundary conditions, Eqs. (3.10) and (3.11):

$$\frac{d\xi_1}{d\zeta} = -\theta\,, \quad \frac{d\xi_c}{d\zeta} = 0, \quad \frac{d\xi_m}{d\zeta} = 0, \quad \frac{d\xi_\sigma}{d\zeta} = 0 \quad \text{at} \quad \zeta = 0 \tag{3.21}$$

In the bulk of solution ($\zeta \to \infty$), all perturbations vanish.

4. Results for the total perturbations

4.1. Basic equations

Under steady-state interfacial expansion, the deviation from equilibrium affects the concentrations of surfactant monomers in the bulk of solution, but only in some vicinity of the interface. The *total* perturbations of ξ_1, ξ_m, ξ_c, and ξ_σ can be defined as integrals:

$$\xi_{i,T} \equiv \int_0^\infty \xi_i(\zeta)\,d\zeta \quad (i = 1, c, m, \sigma) \tag{4.1}$$

The integration of Eqs. (3.15)–(3.20) with respect to ζ, along with the boundary conditions, Eq. (3.21), yields:

$$-\theta\xi_{1,T} - (m_{eq} - w\sigma_{eq})K_s\varphi_{s,T} - \frac{\beta K_m}{m_{eq}}\varphi_{m,T} = -\theta \tag{4.2}$$

$$-\theta\xi_{c,T} + \frac{K_s}{\beta}\varphi_{s,T} = 0 \tag{4.3}$$

$$-\theta\xi_{m,T} - K_s\frac{w m_{eq}}{\beta\sigma_{eq}}\varphi_{s,T} + \frac{K_m}{\sigma_{eq}^2}\varphi_{m,T} = 0 \tag{4.4}$$

$$-\left(\theta + \frac{2K_m}{\sigma_{eq}^2}\right)\xi_{\sigma,T} + K_s(w^2-1)\frac{m_{eq}}{2\beta}\varphi_{s,T} - \frac{K_m}{2\sigma_{eq}^2}\varphi_{m,T} = 0 \tag{4.5}$$

where the integrated (total) reaction fluxes, $\varphi_{s,T}$ and $\varphi_{m,T}$, are:

$$\varphi_{m,T} \equiv \xi_{1,T} - \xi_{m,T} + \frac{\xi_{\sigma,T}}{\sigma_{eq}^2} \tag{4.6}$$

$$\varphi_{s,T} \equiv (m_{eq} - w\sigma_{eq})\xi_{1,T} - m_{eq}\xi_{c,T} + \sigma_{eq}w\xi_{m,T} - (w^2-1)\xi_{\sigma,T} \tag{4.7}$$

In view of Eqs. (4.6)–(4.7), the Eqs. (4.2)–(4.5) form a linear inhomogeneous system of four *algebraic* equations for determining the four total perturbations, $\xi_{1,T}$, $\xi_{m,T}$, $\xi_{c,T}$, and $\xi_{\sigma,T}$. Thus system could be solved by using standard methods. We used the LU decomposition method [47].

4.2. Numerical results and discussion

Numerical results for $\xi_{1,T}(\theta)$, $\xi_{m,T}(\theta)$, $\xi_{c,T}(\theta)$, and $\xi_{\sigma,T}(\theta)$, obtained by solving the linear system of Eqs. (4.2)–(4.5), are given in Fig. 3 for a relatively high micelle concentration, $\beta = (C_{tot} - CMC)/CMC = 100$. In our computations, we assigned typical values to the following constant parameters of the system:

$$m_{eq} = 60, \quad \sigma_{eq} = 5, \quad w = 3, \quad B_m = 0.2 \tag{4.8}$$

The rate constants of the fast and slow processes, K_m and K_s, are varied. To illustrate their influence, we obtained numerical data for the following three values: $K_m/K_s = 10^7$ (Fig. 3a); $K_m/K_s = 10^6$ (Fig. 3b), and $K_m/K_s = 10^5$ (Fig. 3c), at the same $K_m = 10^3$. The perturbation $\xi_{\sigma,T}(\theta)$, which is similar for Fig. 3a–c, is shown only in Fig. 3c.

The general picture in a regular kinetic diagram, Fig. 3, is the following. At high rates of surface deformation (point A in Fig. 3) the total perturbation of the monomer concentration is $\xi_{1,T} \approx 1$, while the other perturbations, $\xi_{c,T}$, $\xi_{m,T}$, and $\xi_{\sigma,T}$, are ≈ 0. In the limit of low deformation rates, $\theta \to 0$, all perturbations become zero. For this reason, $\xi_{c,T}$, $\xi_{m,T}$, and $\xi_{\sigma,T}$ have extremum (sometimes a flat plateau), while $\xi_{1,T}$ monotonically decays with the decrease of θ.

The most important feature of the relaxation curves (Fig. 3) is that $\xi_{m,T}$ merges with $\xi_{1,T}$ at a given point, denoted by B, while $\xi_{c,T}$ merges with $\xi_{1,T}$ (and $\xi_{m,T}$) at another point, denoted by D. The surface deformation rates, corresponding to the points B and D, are denoted by θ_B and θ_D, respectively.

In the regime AB, corresponding to the greatest rates of interfacial deformation ($\theta > \theta_B$), the dynamics of surfactant adsorption is affected by the micellar reaction kinetics. As shown in Section 5.2 below, for the higher micelle concentrations ($\beta > 10$), the effect of the *fast* micellar process is predominant, wile for the lower micelle concentrations ($\beta \approx 1$), the effects of the fast and slow processes become comparable.

As seen in Fig. 3, for $\theta < \theta_B$, we have $\xi_{\sigma,T} \approx 0$ and $\xi_{1,T} \approx \xi_{m,T}$. In view of Eq. (4.6), this means that for $\theta < \theta_B$ the flux of the fast micellar process, $\varphi_{m,T}$, is equal to zero. In other words, for $\theta < \theta_B$ the monomers and micelles are equilibrated with respect to the *fast* micellar process. An expression for estimating θ_B is given by Eq. (5.40) below.

Likewise, Fig. 3 shows that for $\theta < \theta_D$, we have $\xi_{\sigma,T} \approx 0$ and $\xi_{c,T} \approx \xi_{1,T} \approx \xi_{m,T}$. In view of Eq. (4.7), this means that for $\theta < \theta_D$ the flux of the slow micellar process, $\varphi_{s,T}$, is also equal to zero. In other words, for $\theta < \theta_D$ (regime DE) the monomers and micelles are equilibrated with respect to *both* fast and slow micellar processes. Thus, in the regime DE, the dynamics of adsorption occurs under diffusion control, see Eq. (5.46). An expression for estimating θ_D is given by Eq. (5.48).

In the regime BC (Fig. 3), the monomers and micelles are equilibrated with respect to the fast process ($\xi_{m,T} \approx \xi_{1,T}$), but the effect of the slow process is negligible ($\xi_{c,T} \ll \xi_{1,T}$). Then, in the region BC none of the two micellar processes affects the dynamics of adsorption, and, therefore, the latter also happens under diffusion control; see Eq. (5.37) below.

In the regime CD (Fig. 3), again, the monomers and micelles are equilibrated with respect to the fast process ($\xi_{m,T} \approx \xi_{1,T}$), however the effect of the slow process becomes considerable. In other words, in the region CD, the *slow* micellar process affects

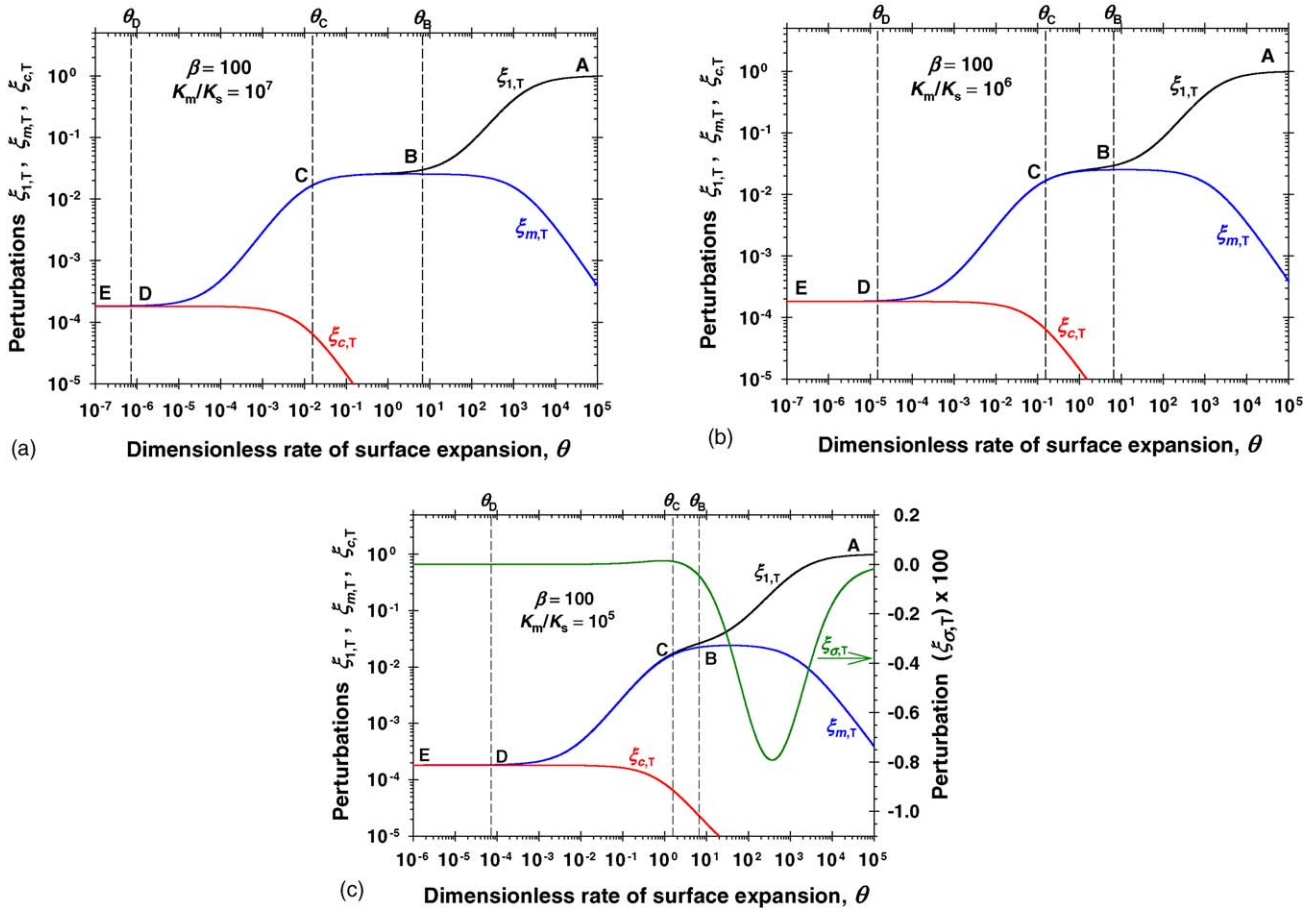

Fig. 3. Total perturbations in monomer concentration, $\xi_{1,T}$, micelle concentration, $\xi_{c,T}$, mean aggregation number, $\xi_{m,T}$, and polydispersity, $\xi_{\sigma,T}$ plotted vs. the dimensionless rate of surface expansion, θ, for $\beta = 100$ and $K_m = 1000$. (a) $K_m/K_s = 10^7$; (b) $K_m/K_s = 10^6$; (c) $K_m/K_s = 10^5$; the other parameters are given by Eq. (4.8). The curves are obtained by numerical solution of the linear system, Eqs. (4.2)–(4.5). $\xi_{\sigma,0}(\theta)$ is similar for (a–c), and is shown only in (c). $\xi_{m,T}$ and $\xi_{1,T}$ merge at the point B; $\xi_{c,T}$ and $\xi_{1,T}$ merge at the point D. θ_B, θ_C and θ_D are the coordinates of the respective points estimated by means of Eqs. (5.40), (5.41) and (5.48).

the dynamics of adsorption. An estimate for the position of the point C, $\theta = \theta_C$, where the effect of the slow process becomes considerable, is given by Eq. (5.41).

The presence of four distinct kinetic regimes, AB, BC, CD, and DE, is a general property of the process of adsorption from micellar solutions. In particular, such regimes are observed in the case of surfactant adsorption at a quiescent interface, reference [22], and at an interface subjected to stationary expansion (the present paper, Fig. 3). Two of these regimes, AB and CD, are affected by the *micellar reaction kinetics*: the rate constants K_m and K_s influence the adsorption kinetics, and consequently, they could be determined by analysis of data for dynamic surface tension and adsorption; see Eqs. (5.5), (5.7), (5.35) and (5.39).

In contrast, the other two regimes, BC and DE correspond to dynamics of adsorption under *diffusion control*. In this case, the dynamic surface tension is not affected by the micellar rate constants K_m and K_s; it can be described as diffusion in a solution of surfactant of apparent diffusion coefficients D_{BC} and D_{DE}. The coefficients D_{BC} and D_{DE} depend on the *equilibrium* micelle concentration, mean aggregation number and polydispersity through the parameters β, m_{eq} and σ_{eq}; see Eqs. (5.38) and (5.47) below.

It should be also noted that in addition to the *regular* kinetic diagrams (Fig. 3 and Section 5) one could sometimes observe *rudimentary* kinetic diagrams (Section 6), characterized by merging or disappearance of the regimes BC and CD.

5. Regular kinetic diagrams: numerical results and analytical expressions

5.1. Numerical results for the subsurface concentration and adsorption

The parameters, which are measured in the experiment, are the interfacial tension γ [26], and the adsorption Γ [27–31]. For small deviations from equilibrium, which are typical for surfactant concentrations above the CMC, the perturbations in γ and Γ are directly related to the perturbation in the subsurface concentration of monomers, $\xi_{1,0} \equiv \xi_1(\zeta = 0)$, see Eq. (3.14). For this reason, in Section 5 we will focus our attention on the calculation of $\xi_{1,0}(\theta)$ and on the investigation of its behavior.

In Section 4, we calculated $\xi_{1,T}(\theta)$ by solving the linear system of algebraic Eqs. (4.2)–(4.5). The problem for calculation of $\xi_{1,0}(\theta)$ is more complicated, because we have to solve a linear

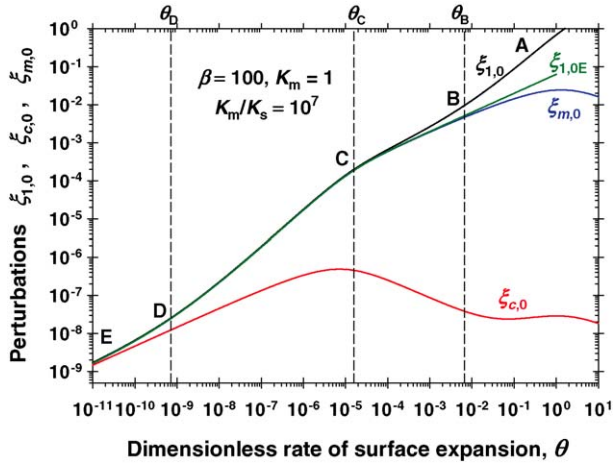

Fig. 4. Perturbations in the subsurface (at $z=0$) monomer concentration, $\xi_{1,0}$, micelle concentration, $\xi_{c,0}$, and mean aggregation number, $\xi_{m,0}$, plotted vs. θ for $\beta=100$, $K_m=1$ and $K_m/K_s=10^7$; the other parameters are given by Eq. (4.8). $\xi_{1,0}$ is proportional to the perturbations in the surface tension and adsorption, see Eq. (3.14). The curves are obtained by numerical solution of the general system of equations in the Appendix A. θ_B, θ_C and θ_D are estimated by means of Eqs. (5.40), (5.41) and (5.48).

system of ordinary differential equations, Eqs. (3.15)–(3.18). For this goal, we used a second-order difference scheme that is described in Appendix A. Illustrative numerical results are plotted in Fig. 4, where the perturbations $\xi_{1,0}(\theta)$, $\xi_{c,0}(\theta)$, and $\xi_{m,0}(\theta)$ are shown. For all of them, the subscript "0" indicates that we are dealing with the subsurface value of the respective perturbation, i.e. with its value at $\zeta=0$.

The kinetic diagram for the subsurface perturbations in Fig. 4 has the same stricture as that for the total perturbations in Fig. 3. Regimes AB, BC, CD, and DE can be identified in the same way as in Section 4, and they have the same physical meaning. Note that in Fig. 3, the merging of $\xi_{m,T}$ and $\xi_{1,T}$ happens at the point B. On the other hand, in Fig. 4 $\xi_{m,0}$ and $\xi_{1,0}$ merge on the left of the point B; the reason for this difference is explained in Section 5.4. The situation with the point D is similar. Below, we consider separately the above regimes, and derive expressions for the dependence $\xi_{1,0}(\theta)$ in each regime. Furthermore, from $\xi_{1,0}(\theta)$ one can determine $\Gamma(\theta)$, and $\gamma(\theta)$ by means of Eq. (3.14).

5.2. Regime AB

The regime AB takes place for sufficiently great rates of surface deformation, i.e. for $\theta>\theta_B$, see Eq. (5.40). In this regime, $\xi_1 \gg \xi_c, \xi_m, \xi_\sigma$. Neglecting the terms with ξ_c, ξ_m, and ξ_σ in Eqs. (3.19) and (3.20), we bring Eq. (3.15) in the form:

$$-\theta\zeta\frac{d\xi_1}{d\zeta} = \frac{d^2\xi_1}{d\zeta^2} - K_{AB}\xi_1 \tag{5.1}$$

$$K_{AB} \equiv (m_{eq} - w\sigma_{eq})^2 K_s + \frac{\beta K_m}{m_{eq}} \tag{5.2}$$

Eq. (5.1) corresponds to stationary convective diffusion, accompanied by a first-order chemical reaction. In fact, every reaction can be described as a first-order reaction in the case of small deviations from equilibrium. For this reason, the model based on equations of the type of Eq. (5.1) is often termed *pseudo-first-order-reaction* (PFOR) model [10,17,20,48].

To find the solution of the problem in the case of stationary convective diffusion, we will use the substitution:

$$\xi_1 \equiv f(y)\sqrt{\theta}\,, \quad y \equiv \zeta\sqrt{\theta} \tag{5.3}$$

then, Eq. (5.1) acquires the form:

$$\frac{d^2 f}{dy^2} + y\frac{df}{dy} - 2a_{AB} f = 0, \quad a_{AB} \equiv \frac{K_{AB}}{2\theta} \tag{5.4}$$

Because equations equivalent to Eq. (5.4) are obtained also for other kinetic regimes, the solution of this equation is considered separately in Section 5.3. Thus, in view of Eqs. (5.3) and (5.18), the solution of Eq. (5.4), along with the boundary condition, Eq. (3.21), is:

$$\xi_{1,0} = \frac{\hat{\Gamma}(0.5 + a_{AB})}{\hat{\Gamma}(1 + a_{AB})}\left(\frac{\theta}{2}\right)^{1/2} \tag{5.5}$$

where $\hat{\Gamma}$ is the known gamma function, $\hat{\Gamma}(x+1) = x\hat{\Gamma}(x)$ [49,50]. Using the fact that $\hat{\Gamma}(0.5) = \pi^{1/2}$ and $\hat{\Gamma}(1) = 1$, we obtain the asymptotic form of Eq. (5.5) for small a_{AB}:

$$\xi_{1,0} = \left(\frac{\pi}{2}\theta\right)^{1/2} \quad (a_{AB} \ll 1) \tag{5.6}$$

Eq. (5.6) is equivalent to Eq. (2.7) that describes diffusion-limited adsorption for concentrations below the CMC; see also Eqs. (3.12) and (3.14). In other words, for $a_{AB} \ll 1$ the effect of the micelles on the adsorption kinetics is negligible.

In the other limiting case, $a_{AB} \gg 1$, the asymptotics of Eq. (5.5) is given by Eq. (5.22), i.e. we have:

$$\xi_{1,0} = \frac{\theta}{\sqrt{K_{AB} + \theta}} \quad (a_{AB} \gg 1, \text{ regime AB}) \tag{5.7}$$

For $K_{AB} \gg \theta$, Eq. (5.7) gives $\xi_{1,0} \propto \theta$, which essentially differs from the square-root dependence in Eq. (5.6).

In general, Eq. (5.5), and its asymptotic form, Eq. (5.7), which characterize the dependence $\xi_{1,0}(\theta)$ in the regime AB, contain the reaction constant K_{AB}, which accounts for the effect of the micelles on the adsorption kinetics. We can express K_{AB} in the form

$$K_{AB} = (1 + R_s)\beta\frac{K_m}{m_{eq}}; \quad R_s \equiv m_{eq}(m_{eq} - w\sigma_{eq})^2\frac{K_s}{\beta K_m} \tag{5.8}$$

where the parameter R_s characterizes the relative importance of the slow micellar process in comparison with the fast one. For the parameter values in Eq. (4.8), we obtain:

$$R_s = 1.215 \times 10^5 \frac{K_s}{\beta K_m} \tag{5.9}$$

Thus, for $K_m/K_s \geq 10^5$ and $\beta=100$ (Figs. 3 and 4), Eq. (5.9) yields $R_s \ll 1$, and the contribution of the slow process is negligible; then R_s could be neglected in Eq. (5.8), and the adsorption kinetics is influenced only by the *fast* micellar process. In contrast, for $K_m/K_s = 10^5$ and $\beta=1$ (low micelle concentration, see

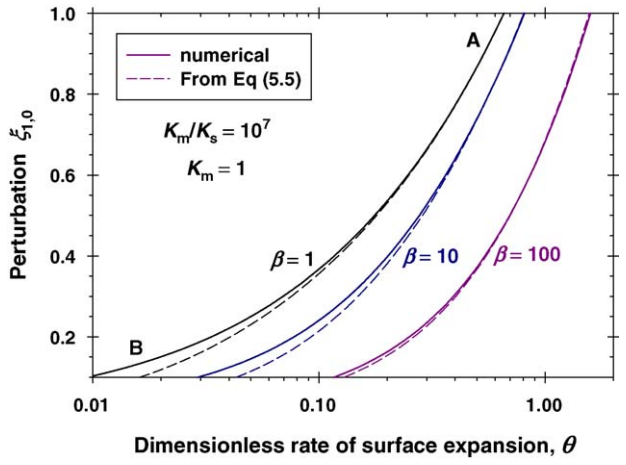

Fig. 5. Plot of the perturbation in the subsurface monomer concentration, $\xi_{1,0}$, vs. θ for θ-values corresponding to the regime AB. The continuous lines represent the exact numerical solution (see the Appendix A), while the dashed lines are obtained from Eq. (5.5). The used parameter values are given in the figure and in Eq. (4.8).

Section 6), Eq. (5.9) yields $R_s \approx 1$, and the contribution of the slow micellar process becomes considerable.

Fig. 5 compares the asymptotic analytical expression, Eq. (5.5) with the exact numerical solution of the system of ordinary differential equations, Eqs. (3.15)–(3.18); see the Appendix A for the numerical procedure. The curves in Fig. 5 show that Eq. (5.5) is very accurate for the larger values of θ. On the other hand, for the smaller θ, where a transition from the regime AB to the regime BC takes place, the accuracy of Eq. (5.5) decreases. Of course, the exact numerical solution (see the Appendix A) describes all kinetic regimes, from AB to DE, and the transitions between them.

5.3. Pseudo-first-order-reaction (PFOR) model

When deriving asymptotic expressions for $\xi_{1,0}(\theta)$ in the different kinetic regimes, the problem is often reduced to the PFOR model for the case of *stationary* diffusion; see e.g. Eq. (5.4). The present section is devoted to the solution of this problem. In general, we consider the equation:

$$\frac{d^2 f}{dy^2} + y\frac{df}{dy} - 2af = 0 \tag{5.10}$$

where a is a positive constant. The solution of Eq. (5.10) has to obey the following boundary conditions:

$$\frac{df}{dy} = -1 \quad \text{at} \quad y = 0 \quad \text{and} \quad f(y) \to 0 \quad \text{at} \quad y \to \infty \tag{5.11}$$

To solve Eq. (5.10), we introduce a new function, $\tilde{f}(y)$, as follows:

$$f(y) \equiv \exp\left(-\frac{y^2}{2}\right)\tilde{f}(y) \tag{5.12}$$

The substitution of Eq. (5.12) into Eq. (5.10) yields the Weber differential equation [51]:

$$\frac{d^2\tilde{f}}{dy^2} - \left(\frac{y^2}{4} + \frac{1}{2} + 2a\right)\tilde{f} = 0 \tag{5.13}$$

Because $\tilde{f}(y) \to 0$ for $y \to \infty$, the solution of Eq. (5.13) can be expressed in terms of the known Whittaker function, U, see chapter 19 in reference [49]:

$$\tilde{f}(y) = XU(b, y), \quad b \equiv 0.5 + 2a \tag{5.14}$$

where X is unknown constant. In view of Eq. (5.12), the substitution of Eq. (5.14) into the boundary condition, Eq. (5.11), yields:

$$\left.\frac{df}{dy}\right|_{y=0} = \left.\frac{d\tilde{f}}{dy}\right|_{y=0} = XU'(b, 0) = -1 \tag{5.15}$$

where the prime denotes first derivative with respect to y. Combining Eqs. (5.12), (5.14) and (5.15), we obtain:

$$f(0) = -\frac{U(b, 0)}{U'(b, 0)} \tag{5.16}$$

Eq. (19.3.5) in [49] gives exact expressions for the functions entering Eq. (5.16):

$$U(b, 0) = \frac{\sqrt{\pi}}{2^{b/2+1/4}\hat{\Gamma}(3/4 + b/2)},$$

$$U'(b, 0) = -\frac{\sqrt{\pi}}{2^{b/2-1/4}\hat{\Gamma}(1/4 + b/2)} \tag{5.17}$$

Finally, we substitute Eq. (5.17) into Eq. (5.16), and take into account that $b = 0.5 + 2a$. As a result, we obtain:

$$f(0, a) = \frac{1}{\sqrt{2}}\frac{\hat{\Gamma}(0.5 + a)}{\hat{\Gamma}(1 + a)} \tag{5.18}$$

Because $\hat{\Gamma}(0.5) = \pi^{1/2}$ and $\hat{\Gamma}(1) = 1$, the asymptotics of Eq. (5.18) for small a is:

$$f(0, a) = (\pi/2)^{1/2} \quad \text{for} \quad a \ll 1 \tag{5.19}$$

To find the asymptotic of $f(0,a)$ for large a, we will use Eq. (6.1.40) in [49]

$$\ln\hat{\Gamma}(z) = \left(z - \frac{1}{2}\right)\ln z - z + \frac{1}{2}\ln(2\pi) + O\left(\frac{1}{z}\right) \tag{5.20}$$

$(1/z \ll 1)$. With the help of the latter expression, one could prove that

$$\ln\frac{\hat{\Gamma}(z)}{\hat{\Gamma}(z + 0.5)} = -\frac{1}{2}(\ln z)\left[1 + O\left(\frac{1}{z\ln z}\right)\right] \tag{5.21}$$

Substituting $z = 0.5 + a$ in the latter expression, and using Eq. (5.18), we derive the asymptotics of $f(0,a)$:

$$f(0, a) \approx \frac{1}{\sqrt{2a + 1}} \quad \text{for} \quad a \gg 1 \tag{5.22}$$

5.4. Region BCDE

By definition, for $\theta<\theta_B$ we have $\xi_1\approx\xi_m$ and $\xi_\sigma\approx0$, see Figs. 3 and 4. Physically, this means that the surfactant monomers and micelles are equilibrated with respect to the fast process. Therefore, we could simplify the general mass-transport problem, Eqs. (3.15)–(3.18). For this goal, we multiply Eq. (3.17) by $\sigma_{eq}^2\beta/m_{eq}$ and sum it up with Eq. (3.15). The result reads:

$$-\theta\zeta\frac{d}{d\zeta}(\xi_1+u\beta\xi_m)=\frac{d^2}{d\zeta^2}(\xi_1+u\beta B_m\xi_m)-m_{eq}K_s\varphi_s \quad (5.23)$$

$$u\equiv\frac{\sigma_{eq}^2}{m_{eq}} \quad (5.24)$$

The boundary condition for Eq. (5.23) requires a special derivation. For this purpose, let us consider a small cylinder of height, L, and bases parallel to the interface. The integration of Eq. (5.23) for $0\le\zeta\le L$, along with the boundary conditions $\partial\xi_1/\partial\zeta=-\theta$ and $\partial\xi_m/\partial\zeta=0$ at $\zeta=0$ (see Eq. (3.21)), yields:

$$\int_0^L d\zeta\left[-\theta\zeta\frac{d}{d\zeta}(\xi_1+u\beta\xi_m)+m_{eq}K_s\varphi_s\right]$$
$$=\frac{d}{d\zeta}(\xi_1+u\beta B_m\xi_m)|_{\zeta=L}+\theta \quad (5.25)$$

Next, in Eq. (5.25) we make the transition $L\to0$ and use the relationship $\xi_m\approx\xi_1$, which is fulfilled in the whole region BCD. Thus, we obtain the boundary condition in the form:

$$(1+u\beta B_m)\frac{d\xi_1}{d\zeta}=-\theta \quad \text{at} \quad \zeta=0 \quad (5.26)$$

In view of Eq. (3.20) for φ_s, the substitution $\xi_\sigma\approx0$ and $\xi_1\approx\xi_m$ in Eqs. (5.23) and (3.16) yields:

$$-(1+u\beta)\theta\zeta\frac{d\xi_1}{d\zeta}=(1+u\beta B_m)\frac{d^2\xi_1}{d\zeta^2}-m_{eq}^2K_s(\xi_1-\xi_c) \quad (5.27)$$

$$-\theta\zeta\frac{d\xi_c}{d\zeta}=B_m\frac{d^2\xi_c}{d\zeta^2}+\frac{m_{eq}K_s}{\beta}(\xi_1-\xi_c) \quad (5.28)$$

The simplified model, based on Eqs. (5.26)–(5.28), is applicable for $\theta<\theta_B$, i.e. for equilibrated *fast* micellar process. This model describes the adsorption dynamics in the whole region BCDE, see Figs. 3 and 4.

The perturbation in the subsurface concentration of surfactant monomers, calculated by means of Eqs. (5.26)–(5.28), is plotted in Fig. 4 and denoted by $\xi_{1,0E}$. One sees that for the smaller values of θ, $\xi_{1,0E}$ coincides with $\xi_{1,0}$, the latter being calculated by the general mathematical procedure in the Appendix A. However, in the vicinity of the point B, $\xi_{1,0E}$ differs from $\xi_{1,0}$. This difference, which originates from the boundary conditions (see below), deserves a special discussion. For this goal, in Fig. 6a we have plotted $\xi_1(\zeta)$ and $\xi_m(\zeta)$ (calculated by using the general procedure; see the Appendix A) for three values of θ corresponding to the region BCD, i.e. for $\theta<\theta_B$; see Fig. 3a.

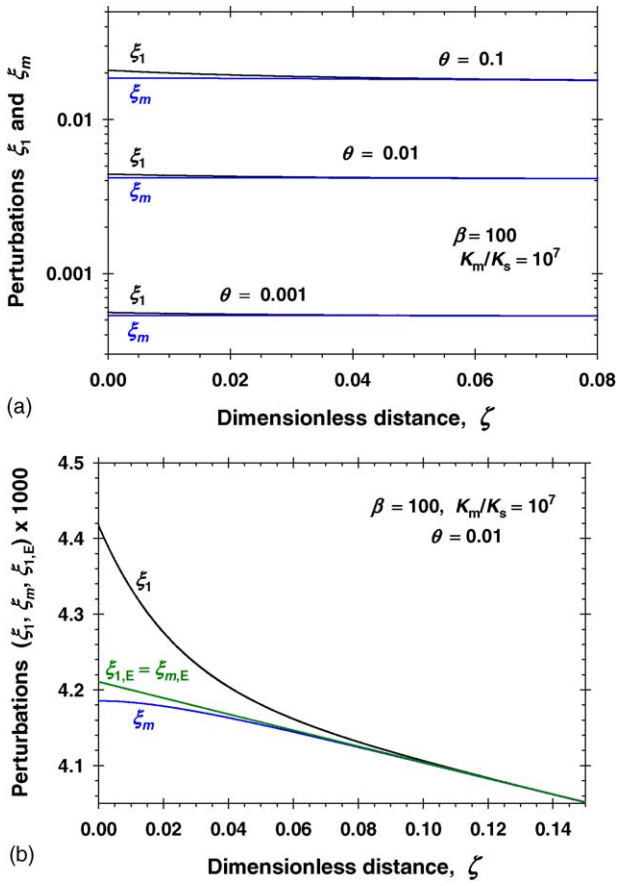

Fig. 6. Dependencies of ξ_1 and ξ_m on the dimensionless distance to the interface, ζ, calculated by using the general procedure in the Appendix A. The parameter values are the same as in Fig. 3a. (a) Plots for three values of θ corresponding to the region BCD, where $\theta<\theta_B$. (b) A magnified plot for $\theta=0.01$; $\xi_{1,E}$ and $\xi_{m,E}$, calculated by the quasi-equilibrium model, Eqs. (5.26)–(5.28), are also shown.

Fig. 6a shows that in the bulk of the solution we really have $\xi_1(\zeta)\equiv\xi_m(\zeta)$. In other words, in the bulk $\varphi_m\equiv0$, i.e. the monomers and micelles are equilibrated with respect to the fast micellar process. However, in the close vicinity of the interface ($\zeta=0$), we have a slight difference between $\xi_1(\zeta)$ and $\xi_m(\zeta)$. This difference is due to the different boundary conditions: $(\partial\xi_1/\partial\zeta)_{\zeta=0}=-\theta$ versus $(\partial\xi_m/\partial\zeta)_{\zeta=0}=0$; i.e. the monomers adsorb (nonzero diffusion flux), but the micelles do not adsorb; see Eq. (3.21).

On the other hand, the simplified model based on Eqs. (5.26)–(5.28) presumes quasi-equilibrium with respect to the fast process, that is $\xi_m(\zeta)\equiv\xi_1(\zeta)$. In such case, $\xi_m(\zeta)$ is no longer independent variable. Then, at the interface we can impose only one boundary condition, for $\xi_1(\zeta)$, and as noted by Joos et al. [9], this must be the condition for the total interfacial mass balance of surfactant. Indeed, the derivation of Eq. (5.26) ensures that the flux of surfactant molecules at the interface must be the same for the "real" system, described by Eqs. (3.15)–(3.21), and for the simplified quasi-equilibrium model, described by Eqs. (5.26)–(5.28). This requirement ensures that the monomer distributions in the "real" and "model" systems coincide in the bulk: As seen in Fig. 6b, in the bulk we really have $\xi_{1E}(\zeta)\equiv\xi_1(\zeta)$. However, close to the interface we have a small difference (about

4%) between $\xi_{1E}(\zeta)$ and $\xi_1(\zeta)$ due to the different boundary conditions.

In conclusion, the correct values of $\xi_{1,0}$ are given by the full model, Eqs. (3.15)–(3.21); see also the Appendix A. The simpler model, Eqs. (5.26)–(5.28), which assumes that $\xi_{1E}(\zeta) \equiv \xi_{mE}(\zeta)$ for every ζ (Fig. 6b), leads to a small difference between $\xi_{1E}(\zeta)$ and $\xi_1(\zeta)$ in the close vicinity of the interface. This is the "price" we pay to work with a simpler model. This difference is the greatest for the subsurface concentrations, $\xi_{1,0E}$ and $\xi_{1,0}$ (at $\zeta = 0$). It disappears for the smaller values of θ, as seen in Fig. 4, or for greater distances from the interface (Fig. 6).

5.5. The regimes BC and CD

The mathematical problem could be further simplified for the region BCD, where $\xi_c \ll \xi_1$, see Figs. 3 and 4. Neglecting the term with ξ_c in Eq. (5.27), we obtain:

$$-(1+u\beta)\theta\zeta\frac{d\xi_1}{d\zeta} = (1+u\beta B_m)\frac{d^2\xi_1}{d\zeta^2} - m_{eq}^2 K_s \xi_1 \tag{5.29}$$

Using the substitutions

$$\xi_1 \equiv f(y)\theta^{1/2}[(1+u\beta)(1+u\beta B_m)]^{-1/2} \tag{5.30}$$

$$\zeta \equiv y\theta^{-1/2}(1+u\beta)^{-1/2}(1+u\beta B_m)^{1/2} \tag{5.31}$$

$$K_{BD} \equiv m_{eq}^2 K_s (1+u\beta)^{-1}, \quad a_{BD} \equiv \frac{K_{BD}}{2\theta} \tag{5.32}$$

we represent Eq. (5.29) and the boundary condition (5.26) in the form:

$$\frac{d^2 f}{dy^2} + y\frac{df}{dy} - 2a_{BD} f = 0 \tag{5.33}$$

$$\frac{df}{dy} = -1 \quad \text{at} \quad y = 0 \tag{5.34}$$

Eqs. (5.33) and (5.34) define a boundary problem, which is equivalent to the PFOR model in Section 5.3. Correspondingly, the solution of this boundary problem is given by Eq. (5.18) with $a = a_{BD}$. Thus, in view of Eq. (5.30), we obtain:

$$\xi_{1,0} = [(1+u\beta)(1+u\beta B_m)]^{-1/2}\frac{\hat{\Gamma}(0.5+a_{BD})}{\hat{\Gamma}(1+a_{BD})}\left(\frac{\theta}{2}\right)^{1/2} \tag{5.35}$$

Using Eq. (5.19), we derive the asymptotics of Eq. (5.35) for small a_{BD}:

$$\xi_{1,0} = [(1+u\beta)(1+u\beta B_m)]^{-1/2} \times (\pi\theta/2)^{1/2} (a_{BD} \ll 1, \text{ regime BC}) \tag{5.36}$$

With the help of Eqs. (3.12) and (3.14), Eq. (5.36) can be expressed in the form of Eq. (2.7):

$$\frac{\Gamma_{eq} - \Gamma}{\Gamma_{eq}} = \left(\frac{\pi\,\dot{\alpha}\,h_a^2}{2D_{BC}}\right)^{1/2} = \left(\frac{\pi\,D_1\,\theta}{2D_{BC}}\right)^{1/2} \text{(regime BC)} \tag{5.37}$$

$$D_{BC} \equiv D_1(1+u\beta)\left(1 + u\beta\frac{D_m}{D_1}\right) \tag{5.38}$$

Here, D_{BC} is an apparent diffusion coefficient. The analogy between Eqs. (2.7) and (5.37) implies that in the regime BC we are dealing with diffusion-limited adsorption. In this regime, the fast micellar process is equilibrated, while the slow micellar process is negligible. For this reason, the rate constants of the two processes, K_m and K_s, do not appear in Eq. (5.37). The apparent diffusivity, D_{BC}, accounts for the presence of micelles through the parameters β, u and D_m; see Eq. (5.24) and (5.38).

Note that Eq. (5.37) is specific for the considered type of dynamics (adsorption at fluid interfaces subjected to *stationary* expansion), while Eq. (5.38) for D_{BC} seems to be universal: it is valid also for other types of interfacial dynamics in regime BC. For example, the same expression for D_{BC} was derived in [22], for adsorption relaxation at a quiescent interface. Comparing experimental data with a simpler model of monodisperse micelles, Joos and van Hunsel [8] obtained a semiempirical expression for D_{BC}, which is equivalent to Eq. (5.38) with $u = 1$. Experimentally, such quadratic dependence of D_{BC} on the micelle concentration, β, has been established for the nonionic surfactant Brij 58 by means of the dynamic drop-volume method [8], and by means of the strip method [9]. The regime BC has been detected also for the surfactant Triton X-100 by means of the maximum-bubble-pressure method [52] for the long times. This regime has been also observed in measurements of dynamic surface tension (or adsorption) for other types of surfactants and experimental methods; see Section 7.

In contrast with the "diffusion-limited" regime BC, in the regime CD the adsorption dynamics is affected by the micellar kinetics through the slow micellar process. In general, the regime CD is described by Eq. (5.35) for $a_{BD} \geq 1$. Note that $a_{BD} \propto K_s$, where, as usual, K_s is the dimensionless rate constant of the slow micellar process; see Eq. (5.32). In particular, the asymptotic form of Eq. (5.35) for $a_{BD} \gg 1$ is:

$$\xi_{1,0} = [(1+\beta u)(1+\beta u B_m)]^{-1/2}\frac{\theta}{\sqrt{K_{BD}+\theta}} \text{ (regime CD)} \tag{5.39}$$

see also Eqs. (5.22) and (5.32). As expected, Eq. (5.39) shows that $\xi_{1,0}$ depends on the rate constant of the slow process, K_s, through K_{BD}, and consequently, K_s could be determined from experimental data for $\xi_{1,0}(\theta,\beta)$ in the regime CD; see also Eq. (3.14).

The boundary between the regimes AB and BC, $\theta = \theta_B$, can be defined as the intersection point of the dependencies $\xi_{1,0}(\theta)$ defined by Eqs. (5.7) and (5.36). Setting equal the right-hand sides of the latter two equations, we obtain:

$$\theta_B = K_{AB}\left[\frac{2}{\pi}(1+u\beta)(1+u\beta B_m) - 1\right]^{-1} \tag{5.40}$$

For $\beta \to 0$ (very low micelle concentrations), the denominator in Eq. (5.40) could become zero and this equation may not give physically meaningful values for θ_B. This reflects the fact that at low micelle concentrations the point B cannot be defined (rudimentary kinetic diagram, see Section 6).

We could define the boundary between the regimes BC and CD, $\theta = \theta_C$, as a point situated between the zones of validity of the asymptotic Eqs. (5.36) and (5.39). An appropriate definition of θ_C could be obtained if we postulate that at $\theta = \theta_C$ the relative deviation of the asymptotic Eq. (5.36) from the exact Eq. (5.35) is 25%. This definition yields:

$$\theta_C = 1.853 K_{BD} = 1.853 m_{eq}^2 K_s (1 + \beta u)^{-1} \tag{5.41}$$

The positions of the points θ_B and θ_C in Figs. 3 and 4 (shown by vertical dashed lines) are determined from Eqs. (5.40) and (5.41). Note that smaller values of K_s lead to wider region BC: compare Fig. 3a–c.

5.6. Regime DE

By definition, for $\theta < \theta_D$ we have $\xi_c \approx \xi_1 \approx \xi_m$ and $\xi_\sigma \approx 0$, see Fig. 3. Physically, this means that the surfactant monomers and micelles are equilibrated with respect to both the fast and slow micellar processes. Consequently, we could simplify the general mass-transport problem, Eqs. (3.15)–(3.18). For this goal, we multiply Eq. (3.16) by βm_{eq} and sum it up with Eq. (5.23). The result reads:

$$-\theta\zeta \frac{d}{d\zeta}(\xi_1 + \beta u \xi_m + \beta m_{eq} \xi_c) = \frac{d^2}{d\zeta^2}(\xi_1 + \beta u B_m \xi_m + \beta m_{eq} B_m \xi_c) \tag{5.42}$$

The boundary condition for Eq. (5.42) can be derived in analogy with the derivation of Eq. (5.26). For this purpose, we first consider a small cylinder of height, L, and bases parallel to the interface. The integration of Eq. (5.42) for $0 \le \zeta \le L$, along with the boundary conditions $\partial\xi_1/\partial\zeta = -\theta$ and $\partial\xi_m/\partial\zeta = \partial\xi_c/\partial\zeta = 0$ at $\zeta = 0$ (see Eq. (3.21)), yields:

$$-\theta \int_0^L d\zeta \zeta \frac{d}{d\zeta}(\xi_1 + u\beta\xi_m + m_{eq}\beta\xi_c) = \frac{d}{d\zeta}(\xi_1 + u\beta B_m \xi_m + m_{eq}\beta B_m \xi_c)|_{\zeta=L} + \theta \tag{5.43}$$

Next, in Eq. (5.43) we make the transition $L \to 0$ and use the relationship $\xi_c = \xi_1 = \xi_m$, which is fulfilled in the region DE. Thus, we obtain the boundary condition in the form:

$$[1 + (m_{eq} + u)\beta B_m] \frac{d\xi_1}{d\zeta} = -\theta \quad \text{at} \quad \zeta = 0 \tag{5.44}$$

The substitution $\xi_c \approx \xi_m \approx \xi_1$ in Eq. (5.42) yields:

$$-[1 + (u + m_{eq})\beta]\theta\zeta \frac{d\xi_1}{d\zeta} = [1 + (u + m_{eq})\beta B_m] \frac{d^2\xi_1}{d\zeta^2} \tag{5.45}$$

Mathematically, the boundary problem, Eqs. (5.44) and (5.45) is analogous to the boundary problem for concentrations below the CMC, Eqs. (2.2) and (2.3), and it can be solved in a similar way. Thus, in view of Eqs. (3.12) and (3.14), an analogue of Eq. (2.7) can be derived for the regime DE:

$$\frac{\Gamma_{eq} - \Gamma}{\Gamma_{eq}} = \xi_{1,0} = \left(\frac{\pi \dot{\alpha} h_a^2}{2 D_{DE}}\right)^{1/2} = \left(\frac{\pi D_1 \theta}{2 D_{DE}}\right)^{1/2} \tag{5.46}$$

$$D_{DE} \equiv D_1[1 + (u + m_{eq})\beta] \left[1 + (u + m_{eq})\beta \frac{D_m}{D_1}\right] \tag{5.47}$$

Here, D_{DE} is an apparent diffusion coefficient. The analogy between Eqs. (2.7) and (5.46) implies that in the regime DE we are dealing with diffusion-limited adsorption. Because in this regime the fast and slow micellar processes are equilibrated, the rate constants of these two processes, K_m and K_s, do not appear in Eqs. (5.46). The latter describes adsorption under purely diffusion control. The apparent diffusivity, D_{DE}, accounts for the presence of micelles through the parameters m_{eq}, β, u and D_m; see Eq. (5.47).

Note that Eq. (5.46) is specific for the considered type of adsorption dynamics (at fluid interfaces subjected to *stationary* expansion), while Eq. (5.47) for D_{DE} seems to be universal: it is valid also for other types of interfacial dynamics in regime DE. For example, the same expression for D_{DE} was derived in [22] for adsorption relaxation at a quiescent interface.

As a rule, $m_{eq} \gg u$, see Eq. (5.24). Then, we can neglect u in Eq. (5.47). The resulting expression for D_{DE} is identical to that obtained by Lucassen [6] in the framework of a simplified model assuming the presence of *monodisperse* micelles of aggregation number m_{eq}. In [6], it was reported that this expression agrees well with experimental data for the adsorption of nonionic surfactants at interfaces of oscillating area.

Because $m_{eq} \gg u$, the dependence $D_{DE}(\beta)$, predicted by Eq. (5.47) is much stronger than the dependence $D_{BC}(\beta)$, predicted by Eq. (5.38). (As usual, $\beta \equiv (C_{tot} - \text{CMC})/\text{CMC}$ is the dimensionless micelle concentration.) The latter fact enables one to easily distinguish between the regimes BC and DE, both of them corresponding to diffusion-limited adsorption: $\Gamma_{eq} - \Gamma \propto \theta^{1/2}$; compare Eqs. (5.37) and (5.46). For example, Joos et al. [8,9,18] established a considerable disagreement between their experimental data and the Lucassen's expression for the apparent diffusivity. The reason is that the data by Joos et al. correspond to the regime BC, while the Lucassen's expression, i.e. Eq. (5.47) with $u = 0$, is derived for the regime DE. (The two regimes have not been distinguished at that time.)

Because the point D is defined as boundary between the regions CD and DE, the boundary point θ_D could be determined as the intersection point of the curves $\xi_{1,0}(\theta)$ defined by Eqs. (5.39) and (5.46). Setting equal the right-hand sides of the latter two equations, one obtains:

$$\theta_D = K_{BD}\left(\frac{2}{\pi}\frac{D_{DE}}{D_{BC}} - 1\right)^{-1} \tag{5.48}$$

where the apparent diffusion coefficients D_{BC} and D_{DE} are defined by Eqs. (5.38) and (5.47); Eq. (5.32) relates K_{BD} to the rate constant of the slow micellar process, K_s. In Figs. 3 and 4, the vertical dashed lines for θ_D are drawn by means of Eq. (5.48).

5.7. Compound asymptotic expression for the whole region ABCDE

R*egular* kinetic diagrams with clearly distinguished regimes AB, BC, CD and DE are observed when $\beta \gg 1$ and

$$\beta K_m \gg (m_{eq} - w\sigma_{eq})^2 m_{eq} K_s \tag{5.49}$$

see the right-hand side of Eq. (5.2). In this case, the values of θ corresponding to the separate regimes differ by order of magnitude, see Figs. 3 and 4. For this reason, one could obtain a compound analytical expression for $\xi_{1,0}(\theta)$ by merely summing up Eq. (5.5) for the regime AB; Eq. (5.35) for the region BCD, and Eq. (5.46) for the regime DE. The resulting expression reads:

$$\xi_{1,0}(\theta) = \left(\frac{\theta}{2}\right)^{1/2} \left[\frac{\hat{\Gamma}(0.5 + a_{AB})}{\hat{\Gamma}(1 + a_{AB})} + \frac{D_1^{1/2}}{D_{BC}^{1/2}} \frac{\hat{\Gamma}(0.5 + a_{BD})}{\hat{\Gamma}(1 + a_{BD})} + \frac{(\pi D_1)^{1/2}}{D_{DE}^{1/2}} \right] \tag{5.50}$$

In view of Eqs. (5.2), (5.4), (5.32) and (5.49), a_{AB} and a_{BD} could be expressed in the form:

$$a_{AB} \approx \frac{K_m \beta}{2 m_{eq} \theta}, \qquad a_{BD} = \frac{K_s m_{eq}^3}{2(m_{eq} + \sigma_{eq}^2 \beta)\theta} \tag{5.51}$$

In view of Eq. (3.14) and (5.50) determines also the dependencies of the surface tension and adsorption on the expansion rate: $\gamma = \gamma(\theta)$ and $\Gamma = \Gamma(\theta)$. We recall that in Eq. (5.50) $\hat{\Gamma}$ denotes the known gamma function (Euler integral of the second kind) [49,50].

In Fig. 7, predictions of the approximate Eq. (5.50) (the dashed lines), are compared against the exact numerical solution described in the Appendix A (the continuous lines). As seen in Fig. 7, the dashed and continuous lines practically coincide. In other words, the approximate analytical expression, Eq. (5.50), is in excellent agreement with the exact numerical solution. We recall that Eq. (5.50) is applicable only in the case of regular kinetic diagrams, for which the relation (5.49) is satisfied.

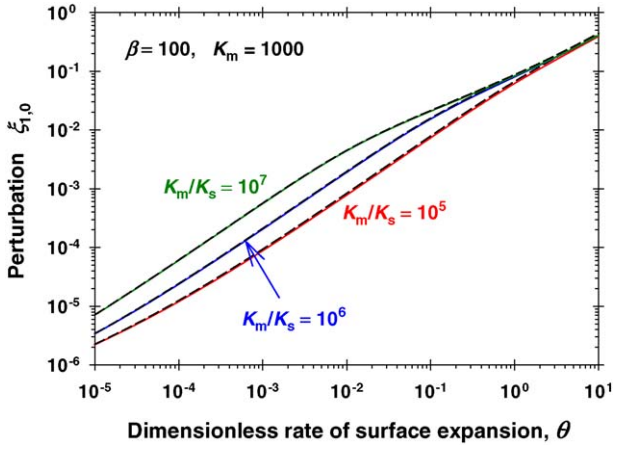

Fig. 7. Plot of $\xi_{1,0}$ vs. θ for three values of K_m/K_s, denoted in the figure; $\beta = 100$, $K_m = 1000$; the other parameter values are given by Eq. (4.8). The dashed and continuous lines, which practically coincide, are, respectively, predictions of the approximate Eq. (5.50) and the exact numerical solution described in the Appendix A. Note that $\xi_{1,0}$ is proportional to the perturbations in the surface tension and adsorption, see Eq. (3.14).

6. Rudimentary kinetic diagrams

The rudimentary kinetic diagrams are characterized by merging or disappearance of the regimes BC and CD when the conditions: (a) $\beta \gg 1$ and (b) $\beta K_m \gg (m_{eq} - w\sigma_{eq})^2 m_{eq} K_s$ are violated; see Eq. (5.49). As a rule, this happens at low micelle concentrations. Below, we consider separately two typical cases.

6.1. Conditions (a) and (b) are both violated

In this case, the points B and C merge with the point D. In other words, the regimes BC and CD are missing. As illustration, in Fig. 8a we have plotted the total perturbations $\xi_{1,T}(\theta)$, $\xi_{m,T}(\theta)$, $\xi_{c,T}(\theta)$, and $\xi_{\sigma,T}(\theta)$, calculated as described in Section 4. The parameter values used in these computations are $\beta = 1$, $K_m = 1$, $K_m/K_s = 10^5$; the other parameters are given by Eq. (4.8). For these parameter values we have:

$$\beta K_m \approx (m_{eq} - w\sigma_{eq})^2 m_{eq} K_s \tag{6.1}$$

Because $\beta = 1$, both the conditions (a) and (b) are violated; see the beginning of Section 6. In Fig. 8a one sees that the curves

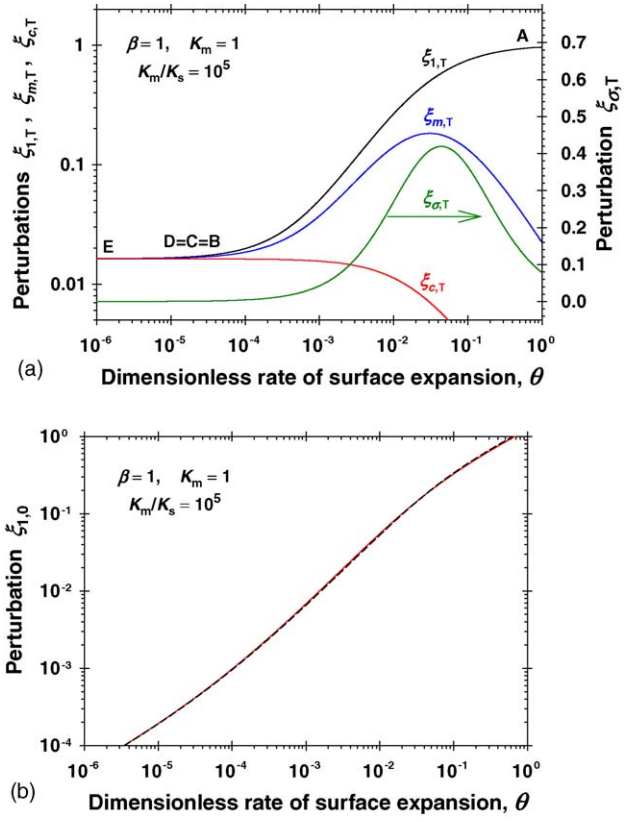

Fig. 8. $K_m/K_s = 10^5$: rudimentary kinetic diagrams at a low micelle concentration, $\beta = 1$. The other parameter values are given by Eq. (4.8) and $K_m = 1$. (a) Plot of $\xi_{1,T}$, $\xi_{c,T}$, $\xi_{m,T}$, and $\xi_{\sigma,T}$ vs. θ. (b) Plot of $\xi_{1,0}$ vs. θ; the dashed and continuous lines, which practically coincide, are, respectively, predictions of the approximate Eq. (6.2) and the exact numerical solution described in the Appendix A.

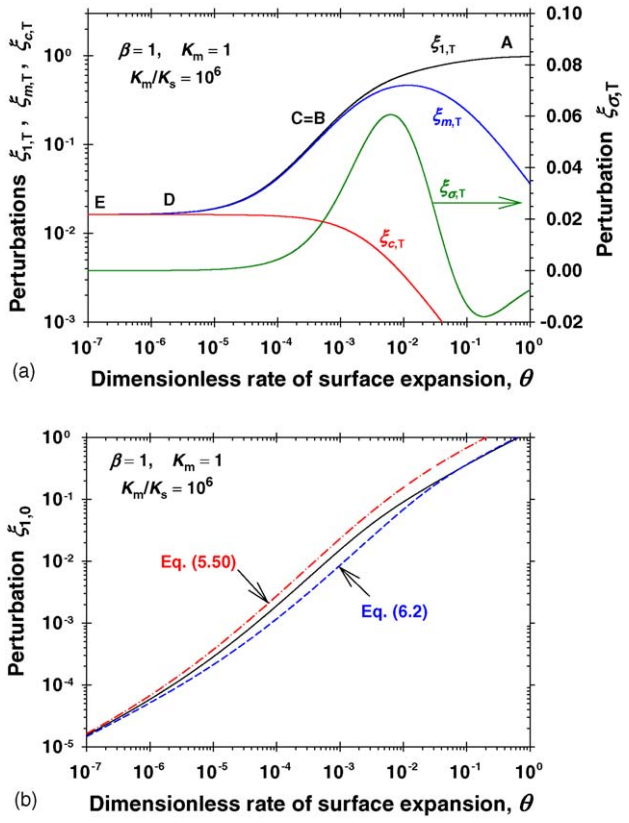

Fig. 9. $K_m/K_s = 10^6$: rudimentary kinetic diagrams at a low micelle concentration, $\beta = 1$. The other parameter values are given by Eq. (4.8) and $K_m = 1$. (a) Plot of $\xi_{1,T}$, $\xi_{c,T}$, $\xi_{m,T}$, and $\xi_{\sigma,T}$ vs. θ. (b) Plot of $\xi_{1,0}$ vs. θ; the dash-dotted, dashed and continuous lines are, respectively, the predictions of Eq. (5.50) and (6.2), and of the exact numerical solution in the Appendix A.

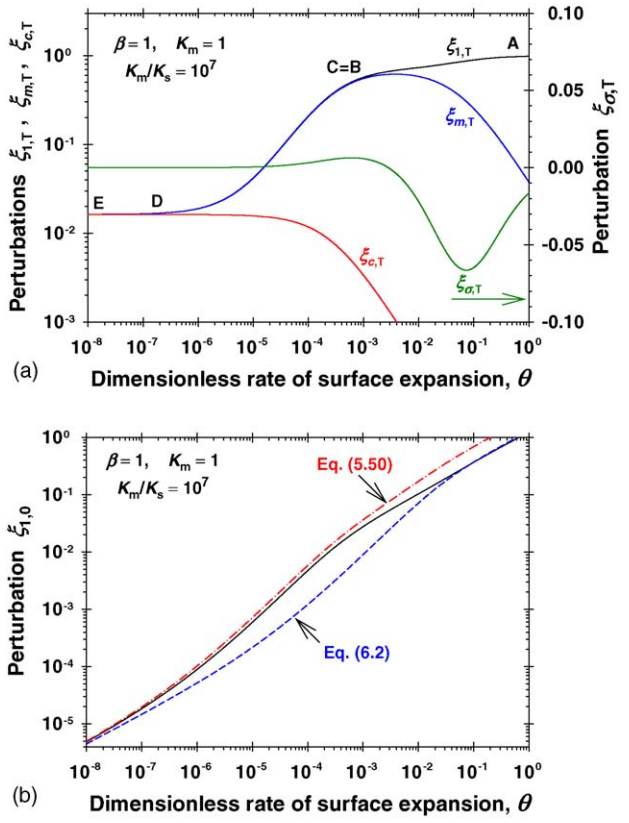

Fig. 10. $K_m/K_s = 10^7$: rudimentary kinetic diagrams at a low micelle concentration, $\beta = 1$. The other parameter values are given by Eq. (4.8) and $K_m = 1$. (a) Plot of $\xi_{1,T}$, $\xi_{c,T}$, $\xi_{m,T}$, and $\xi_{\sigma,T}$ vs. θ. (b) Plot of $\xi_{1,0}$ vs. θ; the dash-dotted, dashed and continuous lines are, respectively, the predictions of Eqs. (5.50) and (6.2), and of the exact numerical solution in the Appendix A.

$\xi_{m,T}(\theta)$ and $\xi_{c,T}(\theta)$ merge with the curve $\xi_{1,T}(\theta)$ practically at the same point. In other words, the points B and D (and the intermediate point C) coincide; compare Fig. 8 with Fig. 3a–c. The latter fact suggests trying an analytical formula for $\xi_{1,0}(\theta)$, obtained from Eq. (5.50) by deleting the term accounting for the region BCD:

$$\xi_{1,0}(\theta) = \left(\frac{\theta}{2}\right)^{1/2} \left[\frac{\hat{\Gamma}(0.5 + a_{AB})}{\hat{\Gamma}(1 + a_{AB})} + \frac{(\pi D_1)^{1/2}}{D_{DE}^{1/2}}\right] \tag{6.2}$$

where a_{AB} is defined by Eqs. (5.2) and (5.4), while D_{DE} is given by Eq. (5.47). In other words, in Eq. (6.2) we keep only the terms corresponding to the regions AB and DE.

In Fig. 8b, we compare the prediction of Eq. (6.2) (dashed line) with the exact numerical solution described in the Appendix A (continuous line). One sees that the dashed and continuous lines coincide, i.e. Eq. (6.2) gives $\xi_{1,0}(\theta)$ very accurately.

6.2. *Only the condition $\beta \gg 1$ is violated*

In this case, the regime BC (diffusion control) is missing, but the regime CD (interfacial dynamics affected by the slow micellar process) is present. As an illustration, in Figs. 9a and 10a we have plotted the total perturbations $\xi_{1,T}(\theta)$, $\xi_{m,T}(\theta)$, $\xi_{c,T}(\theta)$, and $\xi_{\sigma,T}(\theta)$, calculated as described in Section 4. The parameter values are the same as in Fig. 8a, except the ratio K_m/K_s, which is equal to 10^6 and 10^7 for Figs. 9 and 10, respectively. For these parameter values, the relation (5.49) is satisfied. Hence, only the condition $\beta \gg 1$ is violated.

Figs. 9a and 10a indicate that now the points B (merging of $\xi_{1,T}$ and $\xi_{m,T}$) and D (merging of $\xi_{1,T}$ and $\xi_{c,T}$) are well distinct. As in the case of regular kinetic diagrams (Fig. 3), on the left of the point B we have $\xi_{\sigma,T} \approx 0$ and $\xi_{m,T} \approx \xi_{1,T}$. In view of Eq. (4.6), this means that the flux of the fast micellar process, $\varphi_{m,T}$, is equal to zero, and the monomers and micelles are equilibrated with respect to the *fast* micellar process. In addition, on the left of the point D we have $\xi_{\sigma,T} \approx 0$ and $\xi_{c,T} \approx \xi_{1,T} \approx \xi_{m,T}$. This means that on the left of the point D, the flux of the slow micellar process, $\varphi_{s,T}$, is also equal to zero (see Eq. (4.7)), and the monomers and micelles are equilibrated with respect to *both* the fast and slow micellar process. Then, the dynamics of adsorption occurs under diffusion control.

In Figs. 9b and 10b, the exact numerical solution described in the Appendix A (the continuous line) is compared with the predictions of the approximated Eq. (5.50) (the dash-dotted line) and Eq. (6.2) (the dashed line). One sees that in some regions of θ-values, Eqs. (5.50) and (6.2) are close to the exact solution for $\xi_{1,0}(\theta)$, but in other regions there is a considerable difference. For this reason, in the considered case of rudimentary kinetic diagrams it is preferable to use the exact numerical solution.

7. Comparison of theory and experiment

To compare our model with the experiment, and to illustrate its applicability, here we present fits of experimental data published by other authors.

7.1. Dynamic surface tension of Brij 58 measured by the strip method

The dynamic surface tension, γ, of the nonionic surfactant polyoxyethylene-20 hexadecyl ether (Brij 58) has been measured by Li et al. [9] by means of the strip method. It has been established that for each given surfactant concentration the experimental data satisfies the relationship $\gamma - \gamma_{eq} \propto \dot{\alpha}^{1/2}$, where $\dot{\alpha}$ is the surface expansion rate, see Eq. (2.1). In other words, the data indicate adsorption under diffusion control. In addition, Li et al. [9] have established that the apparent diffusivity of the surfactant solution, determined from their data, agrees with an expression equivalent to our Eq. (5.38) with $u = 1$. This finding implies that this set of experimental data corresponds to dynamics of adsorption in the regime BC. Consequently, the data could be interpreted by using the analytical expressions for the regime BC derived in Section 5.5.Combining Eqs. (3.14) and (5.37), we obtain:

$$\gamma - \gamma_{eq} = \frac{\Gamma_{eq}^2 kT}{CMC}\left(\frac{\pi\dot{\alpha}}{2D_{BC}}\right)^{1/2} \tag{7.1}$$

From equilibrium surface-tension data for aqueous solutions of Brij 58 it is known that $CMC = 1.0 \times 10^{-8}$ mol/cm^3 and $\Gamma_{eq} = 2.70 \times 10^{-10}$ mol/cm^2 (at CMC) [9]. Then, from the slope of the experimental plot $\gamma - \gamma_{eq}$ versus $\dot{\alpha}^{1/2}$ for a fixed micellar concentration, β, one can determine the apparent diffusivity of the surfactant solution, $D_{BC}(\beta)$. On the other hand, Eq. (5.38) yields:

$$D_{BC}(\beta) \equiv D_1(1 + u\beta)(1 + uB_m\beta) \tag{7.2}$$

Here, as usual, $\beta = (C_{tot} - CMC)/CMC$; $B_m = D_m/D_1$ is the ratio of the diffusivities of the micelles and monomers. For Brij 58 the value $D_1 \approx 5 \times 10^{-6}$ cm^2/s was used [9].

The points in Fig. 11 represent the data for D_{BC}/D_1 versus β from reference [9]. We fitted these data with parabola, $D_{BC}(\beta)$, in accordance with Eq. (7.2). The best fit yields $B_m = 0.243$ and $u = 1.06$. The latter values are close to those in [9] where $u = 1$ is presumed, and $B_m = 0.25$ is obtained. From our value of $u = \sigma_{eq}^2/m_{eq}$ and the micellar aggregation number, $m_{eq} = 70$ for Brij 58 [53], we calculate the polydispersity of the micelles: $\sigma_{eq} = 8.6$.

The fit of the experimental data in Fig. 11 is very good, and the obtained values of the parameters B_m and σ_{eq} are reasonable. This confirms that the adsorption kinetics in this experiment corresponds to the regime BC. We recall that in this regime, the rate constants of the fast and slow micellar processes, K_m and K_s, do not affect the surfactant adsorption kinetics, and cannot be determined from the fit of the data.

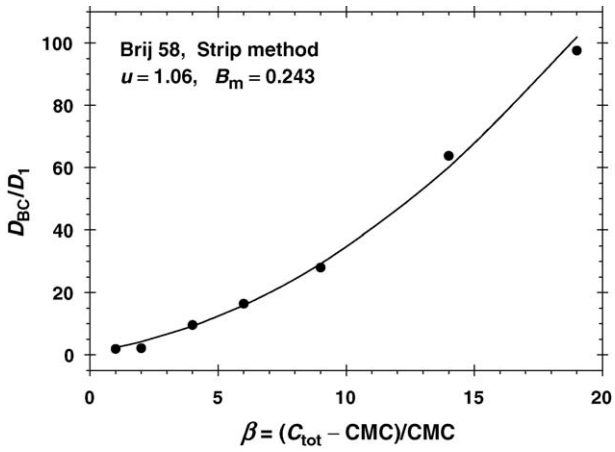

Fig. 11. Plot of the dimensionless apparent diffusion coefficient, D_{BC}/D_1, vs. the dimensionless micelle concentration, β. The points are experimental data for the nonionic surfactant Brij 58 from reference [9]. The continuous line is the best fit by parabola in accordance with Eq. (7.2). The values of u and B_m, determined from the fit, are shown in the figure.

7.2. Dynamic adsorption of C_{14}TAB and C_{16}TAB by the overflowing cylinder method

The overflowing cylinder method allows one to measure directly dynamic adsorption, $\Gamma(\dot{\alpha})$, by ellipsometry [27,30,31], or by neutron reflection [28]. Sets of such experimental data for aqueous solutions of the cationic surfactants tetradecyl- and hexadecyl-thrimethylammonium bromide (C_{14}TAB and C_{16}TAB) have been published in reference [12]; see also [31]. The solutions contain 100 mM electrolyte, NaBr, which suppresses the electrostatic effects. As demonstrated below, it turns out that these data agree well with the kinetic regime BC, like the data for Brij 58 in Section 7.1.

The data in [12] give Γ for various couples of values ($\dot{\alpha}$, β). However, a systematic dependence $\Gamma(\dot{\alpha})$ at fixed β is not available. For this reason, the approach for data interpretation from Section 7.1 cannot be applied. Instead, we will use the following modified approach.Eqs. (5.37) and (5.38) can be represented in the form

$$\Gamma = \Gamma_{eq} - \Gamma_{eq}(\tau_{dif})^{1/2}Y \tag{7.3}$$

$$Y \equiv \left\{\frac{\pi\dot{\alpha}}{[2(1 + u\beta)(1 + u\beta B_m)]}\right\}^{1/2} \tag{7.4}$$

where $\tau_{dif} = h_a{}^2/D_1$ is the characteristic diffusion time of the surfactant monomers. We plotted the experimental data for Γ versus Y in accordance with Eqs. (7.3) and (7.4). The parameters u and B_m, were varied until the best fit of the data by linear regression was achieved (Fig. 12). The intercept of this linear regression, corresponding to $Y = 0$ (i.e. $\dot{\alpha} = 0$), gives the equilibrium adsorption at CMC, Γ_{eq}.

Fig. 12a shows the fit of the data for C_{14}TAB from reference [12], plotted as Γ versus Y; see Eq. (7.3). The best fit corresponds to $B_m = D_m/D_1 = 0.232$ and $u = \sigma_{eq}^2/m_{eq} = 1.2$. The aggregation number of the C_{14}TAB micelles is reported to be $m_{eq} = 80$, in the absence of added electrolyte [53]. Assuming that the addition

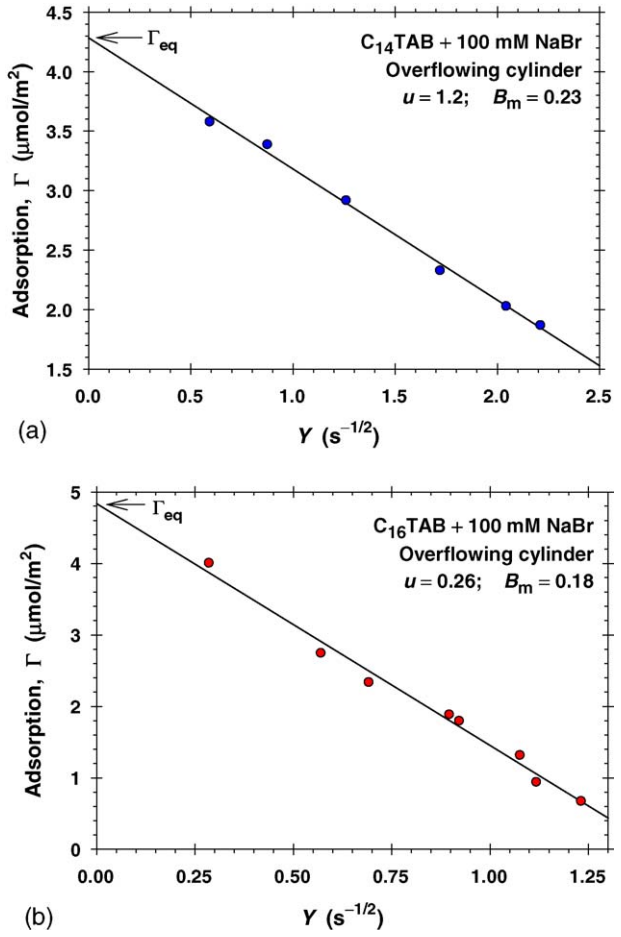

Fig. 12. Plot of the adsorption, Γ, vs. the parameter Y, in accordance with Eqs. (7.3) and (7.4). The points are experimental data for the cationic surfactants (a) C_{14}TAB and (b) C_{16}TAB published in reference [12]. The values of u and B_m, determined from the best linear regression (the straight line), are shown in the figures.

of 100 mM NaBr does not change m_{eq}, from $u = 1.2$ we determine that the polydispersity of the C_{14}TAB micelles is $\sigma_{eq} = 9.8$. The obtained values of B_m and σ_{eq} are reasonable, and the data in Fig. 12a comply well with a straight line, whose intercept gives a realistic value for Γ_{eq}. This agreement between theory and experiment confirms that, in the considered case, the kinetic regime is BC.

Fig. 12b is similar to 12a, but this time the surfactant is C_{16}TAB. The best fit corresponds to $B_m = D_m/D_1 = 0.180$ and $u = \sigma_{eq}^2/m_{eq} = 0.26$. The obtained smaller value of B_m for C_{16}TAB (in comparison with C_{14}TAB) seems reasonable, because C_{16}TAB exhibits a tendency to form larger elongated micelles [54,55]. For a surfactant with hexadecyl chain, the aggregation number of the minimum spherical micelle is about 100 [31,55]. The addition of electrolyte is known to increase the aggregation number of the micelles of ionic surfactants [56,57]. If the aggregation number of C_{16}TAB micelles (for $C_{C16TAB} < 10$ mM) in the presence of 100 mM NaBr is the same as for 100 mM C_{16}TAB without NaBr (because of the same ionic strength), we could use the value $m_{eq} \approx 170$ [53,58]. Then, from $u = 0.26$ we estimate $\sigma_{eq} = 6.7$. The latter value seems somewhat smaller than expected. Nevertheless, the reasonable values of B_m and Γ_{eq} (the latter determined from the intercept of the linear regression in Fig. 12b) indicates that, in the considered case, the kinetic regime is again BC.

7.3. Discussion

The theory developed in this paper is based on linearization for small perturbations; see Section 3.1. Therefore, it is important to estimate the limits of applicability of this linearized theory.

If data for the variation of the surface tension, $\Delta\gamma = \gamma - \gamma_{eq}$ is available as a function of the surface dilatation rate, $\dot{\alpha}$, the simplest way is to plot $\Delta\gamma$ versus $\dot{\alpha}^{1/2}$, as suggested by Li et al. [9], see Fig. 2 therein. For the lower $\dot{\alpha}$, and for the higher surfactant concentrations, the plot of $\Delta\gamma$ versus $\dot{\alpha}^{1/2}$ is linear; this is the region where the linearized theory is applicable. In contrast, for the greater $\dot{\alpha}$, and for the lower surfactant concentrations, a portion of the plot of $\Delta\gamma$ versus $\dot{\alpha}^{1/2}$ may deviate from straight line; this is the region where the linearized theory is not applicable. Fig. 2 in reference [9] represents a good illustrative example.

Alternatively, if data for the variation in the adsorption, Γ, are available, one could plot Γ versus $\dot{\alpha}^{1/2}$ for a given concentration, or Γ versus Y for various concentrations, as in Fig. 12. The linearized theory is valid for the region of not-too-large $\dot{\alpha}$ (or Y), where the respective plot complies with a straight line. For example, for the experimental point with the smallest Γ in Fig. 12, we have $\xi_{1,0} = (\Gamma_{eq} - \Gamma)/\Gamma_{eq} = 0.56$; in other words, $\xi_{1,0}$ is not so small, but nevertheless the linearized theory could be applied (the data agree with a straight line). This could be explained with the fact that the perturbation ξ_1 decays very fast with the distance from the interface, inside the micellar solution.

The above two criteria for validity of the *linearized* theory are applicable when the surfactant transfer takes place under the regime BC; see Eq. (5.37). When the kinetic regime is different, analogous criteria can be obtained from the requirement the experimental data to agree with the kinetic equation of the respective regime. Thus, for the regime AB this is Eq. (5.5), or its asymptotic forms, Eqs. (5.6) and (5.7). For the regime CD this is Eq. (5.39), and for the regime DE this is Eq. (5.46). Note that mathematically Eqs. (5.7) and (5.39) are similar, and one could identify whether the regime is AB or CD from the values of the parameters determined from the fit. Likewise, mathematically Eqs. (5.37) and (5.46) are similar, but one could identify whether the regime is BC or DE from the coefficients D_{BC} and D_{DE} determined from the fit. In general, it is expected that $D_{BC} \ll D_{DE}$, see Eqs. (5.38) and (5.47).

8. Summary and conclusions

Here, we consider a micellar surfactant solution whose surface is subjected to stationary expansion. The adsorption at the fluid interface gives rise to diffusion of surfactant monomers and micelles, and to release of monomers by the micelles. To describe this process, we applied a recently derived general system of four ordinary differential equations, which are linearized for the case of small perturbations, see Eqs. (3.15)–(3.18). The

numerical solution of this problem reveals the existence of four distinct kinetic regimes (Fig. 3). At the greatest expansion rates, the surfactant adsorption is affected by the fast micellar process (regime AB, Section 5.2). At lower expansion rates, the fast process equilibrates and the adsorption occurs under diffusion control (regime BC, Section 5.5). With the further decrease of the expansion rate, the surfactant adsorption is affected by the slow micellar process (regime CD, Eq. (5.39)). Finally, at the lowest expansion rates, both the fast and slow micellar processes are equilibrated, and the adsorption again occurs under diffusion control (regime DE, Section 5.6). For each separate kinetic regime, convenient analytical expressions for the dynamic surface tension and adsorption are derived (Section 5). At low micelle concentrations, "rudimentary" kinetic diagrams are observed, which are characterized by merging or disappearance of the regimes BC and CD (Section 6). Usually, only one of the kinetic regimes is experimentally detected. The developed theoretical model enables one to identify which of the four regimes is observed in a given experiment, and to interpret properly the obtained data for the dynamic surface tension and/or adsorption. We applied the model to process available data from references [9,12] for the nonionic surfactant Brij 58, and for two cationic surfactants (C_{14}TAB and C_{16}TAB); see Section 7. Good agreement between theory and experiment is achieved (Figs. 11 and 12), which implies that the kinetic regime is BC in the considered specific cases.

Acknowledgement

This work was supported by Unilever Research & Development, Connecticut, USA.

Appendix A. Numerical procedure for solution of the boundary problem (3.15)–(3.21)

At the first step, we introduce a convenient new scaling of the normal coordinate, ζ, and of the perturbations, ξ_1, ξ_c, ξ_m and ξ_σ, as follows:

$$\zeta = \tilde{\zeta}\theta^{-1/2}, \quad \xi_i \equiv \tilde{\xi}_i\theta^{1/2} \quad (i = 1, c, m, \sigma) \tag{A.1}$$

The substitution of Eq. (A.1) into Eqs. (3.15)–(3.18), yields:

$$-\tilde{\zeta}\frac{d\tilde{\xi}_1}{d\tilde{\zeta}} = \frac{d^2\tilde{\xi}_1}{d\tilde{\zeta}^2} - (m_{eq} - w\sigma_{eq})\frac{K_s}{K_m\tilde{\theta}}\tilde{\varphi}_s - \frac{\beta}{m_{eq}\tilde{\theta}}\tilde{\varphi}_m \tag{A.2}$$

$$-\tilde{\zeta}\frac{d\tilde{\xi}_c}{d\tilde{\zeta}} = B_m\frac{d^2\tilde{\xi}_c}{d\tilde{\zeta}^2} + \frac{K_s}{\beta K_m\tilde{\theta}}\tilde{\varphi}_s \tag{A.3}$$

$$-\tilde{\zeta}\frac{d\tilde{\xi}_m}{d\tilde{\zeta}} = B_m\frac{d^2\tilde{\xi}_m}{d\tilde{\zeta}^2} - \frac{K_s}{K_m\tilde{\theta}}\frac{wm_{eq}}{\beta\sigma_{eq}}\tilde{\varphi}_s + \frac{1}{\sigma_{eq}^2\tilde{\theta}}\tilde{\varphi}_m \tag{A.4}$$

$$-\tilde{\zeta}\frac{d\tilde{\xi}_\sigma}{d\tilde{\zeta}} = B_m\frac{d^2\tilde{\xi}_\sigma}{d\tilde{\zeta}^2} + \frac{K_s}{K_m\tilde{\theta}}(w^2-1)\frac{m_{eq}}{2\beta}\tilde{\varphi}_s - \frac{1}{2\sigma_{eq}^2\tilde{\theta}}\tilde{\varphi}_m - \frac{2}{\sigma_{eq}^2\tilde{\theta}}\tilde{\xi}_\sigma \tag{A.5}$$

where $\tilde{\theta} = \theta/K_m$, and the rescaled fluxes, $\tilde{\varphi}_s$ and $\tilde{\varphi}_m$, are defined by expressions analogous to Eqs. (3.19)–(3.20):

$$\tilde{\varphi}_m \equiv \tilde{\xi}_1 - \tilde{\xi}_m + \frac{\tilde{\xi}_\sigma}{\sigma_{eq}^2} \tag{A.6}$$

$$\tilde{\varphi}_s \equiv (m_{eq} - w\sigma_{eq})\tilde{\xi}_1 - m_{eq}\tilde{\xi}_c + w\sigma_{eq}\tilde{\xi}_m - (w^2-1)\tilde{\xi}_\sigma \tag{A.7}$$

The boundary condition (3.21) is transformed in a universal form, which does not contain θ:

$$\frac{d\tilde{\xi}_1}{d\tilde{\zeta}} = -1\,, \quad \frac{d\tilde{\xi}_c}{d\tilde{\zeta}} = 0, \quad \frac{d\tilde{\xi}_m}{d\tilde{\zeta}} = 0, \quad \frac{d\tilde{\xi}_\sigma}{d\tilde{\zeta}} = 0 \text{ at } \tilde{\zeta} = 0 \tag{A.8}$$

To solve numerically the boundary problem (A.2)–(A.8), one has to specify the values of the following input parameters: (i) parameters related to the equilibrium micellar solution: β, m_{eq}, σ_{eq}, and w; (ii) diffusion and kinetic parameters: B_m and K_m/K_s; and (iii) the dimensionless interfacial expansion rate, $\tilde{\theta}$. It is important to note that the boundary problem (A.2)–(A.8) does not contain the characteristic diffusion time, $\tau_{dif} = h_a^2/D_1$. In particular, we have $K_m/K_s = k_m^-/k_S^-$, and $\tilde{\theta} = \dot{\alpha}/k_m^-$; see Eq. (4.1). Moreover, to solve this dimensionless boundary problem, we have not to introduce the absolute value of k_m^- or K_m.

The solution of this problem yields the dependencies $\tilde{\xi}_{i,0}(\tilde{\theta})$ and $\tilde{\xi}_{i,T}(\tilde{\theta})$. To obtain the kinetic diagrams of $\xi_{i,0}(\theta)$ and $\xi_{i,T}(\theta)$, like those in Figs. 3, 4 and 7–10, one has to specify the value of K_m. Because, these diagrams are given in double-logarithmic scale, it is convenient to present the relations between the two types of variables in the form:

$$\log\,\theta = \log\,\tilde{\theta} + \log\,K_m \tag{A.9}$$

$$\log\,\xi_{i,0} = \log[\tilde{\xi}_{i,0}(\tilde{\theta})\tilde{\theta}^{1/2}] + \frac{1}{2}\log\,K_m \tag{A.10}$$

(i = 1,c,m,σ). In addition, $\tilde{\xi}_{i,T} = \xi_{i,T}$, see Eqs. (4.1) and (A.1). Note that $\log K_m$ enters Eqs. (A.9) and (A.10) as an additive term. Consequently, the variation of $K_m \equiv k_m^-\tau_{dif}$ (or the separate variations of k_m^- and τ_{dif}) leads only to a simple *translation* of the curves $\xi_{i,0}(\theta)$ and $\xi_{i,T}(\theta)$ (in Figs. 3, 4 and 7–10), without changes in their shape. In the case of $\xi_{i,T}(\theta)$, the translation is only along the horizontal axis.

As mentioned in Section 3, the interfacial expansion creates a perturbation in the bulk of solution. Under steady-state conditions, the penetration depth of this perturbation depends on the rate of surface expansion, θ. However, in terms of the new variables, defined by Eq. (A.1), θ disappears from the boundary conditions; compare Eqs. (3.21) and (A.8). For this reason, in terms of $\tilde{\zeta}$, the penetration depth of the perturbation is universal and decays as $\exp(-\tilde{\zeta}^2/2)$. Consequently, the width of the integration domain, $0 \le \tilde{\zeta} \le \tilde{\zeta}_\infty$, determined by $\tilde{\zeta}_\infty$, can be fixed in a universal manner, irrespective of the specific value of θ. In our computations, we chose $\tilde{\zeta}_\infty = 7$. Indeed, for $\tilde{\zeta}_\infty = 7$ we have $\exp(-\tilde{\zeta}_\infty^2/2) = 2.3 \times 10^{-11}$, and consequently, all perturbations are practically zero for depth $\tilde{\zeta} > 7$.

To solve the boundary problem (A.2)–(A.8), we divided the numerical domain, $[0, \tilde{\zeta}_\infty]$, on N equal intervals of endpoints $\tilde{\zeta}_0, \tilde{\zeta}_1, \tilde{\zeta}_2, \ldots, \tilde{\zeta}_N$, with step $\Delta\tilde{\zeta} = \tilde{\zeta}_\infty/N$. We used a second order difference scheme [47]; the first and second derivatives in the bulk are computed as follows:

$$\frac{\mathrm{d}f}{\mathrm{d}\tilde{\zeta}} = \frac{f(\tilde{\zeta}+\Delta\tilde{\zeta}) - f(\tilde{\zeta}-\Delta\tilde{\zeta})}{2\Delta\tilde{\zeta}}, \quad \frac{d^2 f}{\mathrm{d}\tilde{\zeta}^2} = \frac{f(\tilde{\zeta}+\Delta\tilde{\zeta}) - 2f(\tilde{\zeta}) + f(\tilde{\zeta}-\Delta\tilde{\zeta})}{(\Delta\tilde{\zeta})^2} \tag{A.11}$$

In the boundary condition (A.8), the second order forward difference scheme is used for the first derivative [47]:

$$\frac{\mathrm{d}f}{\mathrm{d}\tilde{\zeta}} = \frac{-3f(\tilde{\zeta}) + 4f(\tilde{\zeta}+\Delta\tilde{\zeta}) - f(\tilde{\zeta}+2\Delta\tilde{\zeta})}{2\Delta\tilde{\zeta}} \tag{A.12}$$

With the help of Eqs. (A.11) and (A.12), the boundary problem (A.2)–(A.8) is reduced to a linear system of equations. The values of functions in the discrete nodes $0, \tilde{\zeta}_1, \tilde{\zeta}_2, \ldots, \tilde{\zeta}_N$ are ordered as $\tilde{\xi}_1(0)$, $\tilde{\xi}_c(0)$, $\tilde{\xi}_m(0)$, $\tilde{\xi}_\sigma(0)$; $\tilde{\xi}_1(\tilde{\zeta}_1)$, $\tilde{\xi}_c(\tilde{\zeta}_1)$, $\tilde{\xi}_m(\tilde{\zeta}_1)$, $\tilde{\xi}_\sigma(\tilde{\zeta}_1)$, etc. This procedure reduces the considered system of equations to a system with eight upper and lower diagonals, which is solved using the generalized Thomas algorithm [47]. Our calculations have been carried out at $N = 400{,}000$, which gives a very high accuracy of the obtained numerical results: the error in the numerical scheme is of the order of $(\Delta\tilde{\zeta})^2 = 3.06 \times 10^{-10}$.

References

[1] G.C. Kresheck, E. Hamory, G. Davenport, H.A. Scheraga, Determination of the dissociation rate of dodecylpyridinium iodide micelles by a temperature-jump technique, J. Am. Chem. Soc. 88 (1966) 246–253.

[2] E.A.G. Aniansson, S.N. Wall, On the kinetics of step-wise micelle association, J. Phys. Chem. 78 (1974) 1024–1030.

[3] R. Zana (Ed.), Dynamics of Surfactant Self-Assemblies, CRC Press, Boca Raton, 2005.

[4] B.A. Noskov, D.O. Grigoriev, Adsorption from micellar solutions, in: V.B. Fainerman, D. Möbius, R. Miller (Eds.), Surfactants: Chemistry, Interfacial Properties, Applications, Elsevier, Amsterdam, 2001, pp. 401–509.

[5] B.A. Noskov, Kinetics of adsorption from micellar solutions, Adv. Colloid Interface Sci. 95 (2002) 237–293.

[6] J. Lucassen, Adsorption kinetics in micellar systems, Faraday Discuss. Chem. Soc. 59 (1975) 76–87.

[7] J. Lucassen, D. Giles, Dynamic surface properties of nonionic surfactant solutions, J. Chem. Soc. Faraday Trans. I 71 (1975) 217–232.

[8] P. Joos, J. van Hunsel, Adsorption kinetics of micellar Brij 58 solutions, Colloids Surf. A 33 (1988) 99–108.

[9] B. Li, P. Joos, M. van Uffelen, Adsorption kinetics of Brij 58 micellar solution, J. Colloid Interface Sci. 171 (1995) 270–275.

[10] P. Joos, Dynamic Surface Phenomena, VSP BV, AH Zeist, The Netherlands, 1999.

[11] R. Miller, Adsorption kinetics of surfactants from micellar solutions, Colloid Polymer Sci. 259 (1981) 1124–1128.

[12] C.J.W. Breward, P.D. Howell, Straining flow of a micellar surfactant solution, Eur. J. Appl. Math. 15 (2004) 511–531.

[13] K.D. Danov, P.M. Vlahovska, T.S. Horozov, C.D. Dushkin, P.A. Kralchevsky, A. Mehreteab, G. Broze, Adsorption from micellar surfactant solutions: nonlinear theory and experiment, J. Colloid Interface Sci. 183 (1996) 223–235.

[14] B.A. Noskov, Diffusion of micellar surfactants in liquids. The influence of the fast relaxation process, Kolloidn. Zh. 52 (1990) 509–514.

[15] A. Johner, J.F. Joanny, Block copolymer adsorption in a selective solvent: a kinetic study, Macromolecules 23 (1990) 5299–5311.

[16] C.D. Dushkin, I.B. Ivanov, Effects of the polydispersity of diffusing micelles on the dynamic surface elasticity, Colloids Surf. 60 (1991) 213–233.

[17] C.D. Dushkin, I.B. Ivanov, P.A. Kralchevsky, The kinetics of the surface tension of micellar surfactant solutions, Colloids Surf. 60 (1991) 235–261.

[18] J. van Hunsel, G. Bleys, P. Joos, Adsorption kinetics at the oil/water interface, J. Colloid Interface Sci. 114 (1986) 432–441.

[19] G. Geeraerts, P. Joos, Dynamic surface tension of micellar Triton X-100 solutions, Colloids Surf. A 90 (1994) 149–154.

[20] K.D. Danov, D.S. Valkovska, P.A. Kralchevsky, Adsorption relaxation for nonionic surfactants under mixed barrier-diffusion and micellization-diffusion control, J. Colloid Interface Sci. 251 (2002) 18–25.

[21] K.D. Danov, P.A. Kralchevsky, N.D. Denkov, K.P. Ananthapadmanabhan, A. Lips, Mass transport in micellar surfactant solutions. 1. Relaxation of micelle concentration, aggregation number and polydispersity, Adv. Colloid Interface Sci. 119 (2006), in press.

[22] K.D. Danov, P.A. Kralchevsky, N.D. Denkov, K.P. Ananthapadmanabhan, A. Lips, Mass transport in micellar surfactant solutions. 2. Theoretical modeling of adsorption at a quiescent interface, Adv. Colloid Interface Sci. 119 (2006), in press.

[23] T. Horozov, L. Arnaudov, A novel fast technique for measuring dynamic surface and interfacial tension of surfactant solutions at constant interfacial area, J. Colloid Interface Sci. 219 (1999) 99–109.

[24] T. Horozov, L. Arnaudov, Adsorption kinetics of some polyethylene glycol octylphenyl ethers studied by the fast formed drop technique, J. Colloid Interface Sci. 222 (2000) 146–155.

[25] R. van den Bogaert, P. Joos, Dynamic surface tensions of sodium myristate solutions, J. Phys. Chem. 83 (1979) 2244–2248.

[26] E. Rillaerts, P. Joos, Measurements of the dynamic surface tension and surface dilatational viscosity of adsorbed mixed monolayers, J. Colloid Interface Sci. 88 (1982) 1–7.

[27] S. Manning-Benson, C.D. Bain, R.C. Darton, Measurement of dynamic interfacial properties in an overflowing cylinder by ellipsometry, J. Colloid Interface Sci. 189 (1997) 109–116.

[28] S. Manning-Benson, S.W.R. Parker, C.D. Bain, J. Penfold, Measurement of the dynamic surface excess in an overflowing cylinder by neutron reflection, Langmuir 14 (1998) 990–996.

[29] C.D. Bain, S. Manning-Benson, R.C. Darton, Rates of mass transfer and adsorption of hexadecyltrimethylammonium bromide at an expanding air–water interface, J. Colloid Interface Sci. 229 (2000) 247–256.

[30] T. Battal, G.C. Shearman, D.S. Valkovska, C.D. Bain, R.C. Darton, J. Eastoe, Determination of the dynamic surface excess of a homologous series of cationic surfactants by ellipsometry, Langmuir 19 (2003) 1244–1248.

[31] D.S. Valkovska, G.C. Shearman, C.D. Bain, R.C. Darton, J. Eastoe, Adsorption of ionic surfactants at an expanding air–water interface, Langmuir 20 (2004) 4436–4445.

[32] S. Sugden, The determination of surface tension from the maximum pressure in bubbles, J. Chem. Soc. 121 (1922) 858–866;
S. Sugden, The determination of surface tension from the maximum pressure in bubbles, J. Chem. Soc. 125 (1924) 27–31.

[33] T.S. Horozov, C.D. Dushkin, K.D. Danov, L.N. Arnaudov, O.D. Velev, A. Mehreteab, G. Broze, Effect of the surface expansion and wettability of capillary on the dynamic surface tension measured by maximum bubble pressure method, Colloids Surf. A 113 (1996) 117–126.

[34] N.A. Mishchuk, S.S. Dukhin, V.B. Fainerman, V.I. Kovalchuk, R. Miller, Hydrodynamic processes in dynamic bubble pressure experiments. Part 5. The adsorption at the surface of a growing bubble, Colloids Surf. A 192 (2001) 157–175.

[35] V.B. Fainerman, V.N. Kazakov, S.V. Lylyk, A.V. Makievski, R. Miller, Dynamic surface tension measurements of surfactant solutions using the maximum bubble pressure method—limits of applicability, Colloids Surf. A 250 (2004) 97–102.

[36] R.L. Kao, D.A. Edwards, D.T. Wasan, E. Chen, Measurement of the dynamic interfacial tension and interfacial dilatational viscosity at high rates of interfacial expansion using the maximum bubble pressure method. II. Liquid–liquid interface, J. Colloid Interface Sci. 148 (1992) 257–260.
[37] R. Nagarajan, D.T. Wasan, Measurement of dynamic interfacial tension by an expanding drop tensiometer, J. Colloid Interface Sci. 159 (1993) 164–173.
[38] D.O. Johnson, K.J. Stebe, Experimental confirmation of the oscillating bubble technique with comparison to the pendant bubble method: the adsorption dynamics of 1-decanol, J. Colloid Interface Sci. 182 (1996) 526–538.
[39] H. Fruhner, K.D. Wantke, A new oscillating bubble technique for measuring surface dilational properties, Colloid Surf. A 114 (1996) 53–59.
[40] V.I. Kovalchuk, J. Krägel, E.V. Aksenenko, G. Loglio, L. Liggieri, Oscillating bubble and drop techniques, in: D. Möbius, R. Miller (Eds.), Novel Methods to Study Interfacial Layers, Elsevier, Amsterdam, 2001, pp. 485–516.
[41] V.I. Kovalchuk, J. Krägel, A.V. Makievski, F. Ravera, L. Liggieri, G. Loglio, V.B. Fainerman, R. Miller, Rheological surface properties of C_{12}DMPO solution as obtained from amplitude- and phase-frequency characteristics of an oscillating bubble system, J. Colloid Interface Sci. 280 (2004) 498–505.
[42] P.A. Kralchevsky, Micromechanical description of curved interfaces, thin films and membranes, J. Colloid Interface Sci. 137 (1990) 217–233.
[43] F. Van Voorst Vader, Th.F. Erkens, M. van den Tempel, Measurement of dilatational surface properties, Trans. Faraday Soc. 60 (1964) 1170–1177.
[44] P.A. Kralchevsky, Y.S. Radkov, N.D. Denkov, Adsorption from surfactant solutions under diffusion control, J. Colloid Interface Sci. 161 (1993) 361–365.
[45] C.J.W. Breward, R.C. Darton, P.D. Howell, J.R. Ockendon, The effect of surfactants on expanding free surfaces, Chem. Eng. Sci. 56 (2001) 2867–2878.
[46] P.D. Howell, C.J.W. Breward, Mathematical modeling of the overflowing cylinder experiment, J. Fluid Mech. 474 (2003) 275–298.
[47] W.H. Press, S.A. Teukolsky, W.T. Vetterling, B.P. Flannery, Numerical Recipes in FORTRAN. The Art of Scientific Computing, second ed., Cambridge University Press, Cambridge, 1992.
[48] S.S. Dukhin, G. Kretzschmar, R. Miller, Dynamics of Adsorption at Liquid Interfaces, Elsevier, Amsterdam, 1995.
[49] M. Abramowitz, I.A. Stegun (Eds.), Handbook of Mathematical Functions, Dover, New York, 1974.
[50] G.A. Korn, T.M. Korn, Mathematical Handbook for Scientists and Engineers, second ed., Dover, New York, 2000.
[51] E.T. Whittaker, G.N. Watson, A Course in Modern Analysis, fourth ed., Cambridge University Press, Cambridge, England, 1990.
[52] A.V. Makievski, V.B. Fainerman, P. Joos, Dynamic surface tension of micellar Triton X-100 solutions by the maximum-bubble-pressure method, J. Colloid Interface Sci. 166 (1994) 6–13.
[53] Sigma/Aldrich, Detergents Properties and Applications, Published online: www.sigmaaldrich.com/img/assets/15402/Detergent_Selection_Table.pdf.
[54] F. Reiss-Husson, V. Luzzati, The structure of the micellar solutions of some amphiphilic compounds in pure water as determined by absolute small-angle X-ray scattering techniques, J. Phys. Chem. 68 (1964) 3504–3511.
[55] R. Zana, H. Lévy, D. Danino, Y. Talmon, K. Kwetkat, Mixed micellization of cetyltrimethylammonium bromide and an anionic dimeric (gemini) surfactant in aqueous solution, Langmuir 13 (1997) 402–408.
[56] P.J. Missel, N.A. Mazer, G.B. Benedek, C.Y. Young, M.C. Carey, Thermodynamic analysis of the growth of sodium dodecyl sulfate micelles, J. Phys. Chem. 84 (1980) 1044–1057.
[57] R.G. Alargova, K.D. Danov, P.A. Kralchevsky, G. Broze, A. Mehreteab, Growth of giant rodlike micelles of ionic surfactant in the presence of Al^{3+} counterions, Langmuir 14 (1998) 4036–4049.
[58] O.R. Pal, V.G. Gaikar, J.V. Joshi, P.S. Goyal, V.K. Aswal, Small-angle neutron scattering studies of mixed cetyl trimethylammonium bromide–buthyl benzene sulfonate solutions, Langmuir 18 (2002) 6764–6768.